

Learning Deep Kernels for Non-Parametric Two-Sample Tests

Feng Liu^{*12} Wenkai Xu^{*2} Jie Lu¹ Guangquan Zhang¹ Arthur Gretton² D. J. Sutherland³

Abstract

We propose a class of kernel-based two-sample tests, which aim to determine whether two sets of samples are drawn from the same distribution. Our tests are constructed from kernels parameterized by deep neural nets, trained to maximize test power. These tests adapt to variations in distribution smoothness and shape over space, and are especially suited to high dimensions and complex data. By contrast, the simpler kernels used in prior kernel testing work are spatially homogeneous, and adaptive only in lengthscale. We explain how this scheme includes popular classifier-based two-sample tests as a special case, but improves on them in general. We provide the first proof of consistency for the proposed adaptation method, which applies both to kernels on deep features and to simpler radial basis kernels or multiple kernel learning. In experiments, we establish the superior performance of our deep kernels in hypothesis testing on benchmark and real-world data. The code of our deep-kernel-based two sample tests is available at github.com/fengliliu90/DK-for-TST.

1. Introduction

Two sample tests are hypothesis tests aiming to determine whether two sets of samples are drawn from the same distribution. Traditional methods such as t -tests and Kolmogorov-Smirnov tests are mainstays of statistical applications, but require strong parametric assumptions about the distributions being studied and/or are only effective on data in ex-

tremely low-dimensional spaces. A broad set of recent work in statistics and machine learning has focused on relaxing these assumptions, with methods either generally applicable or specific to various more complex domains (Gretton et al., 2012a; Székely & Rizzo, 2013; Heller & Heller, 2016; Jitkrittum et al., 2016; Ramdas et al., 2017; Lopez-Paz & Oquab, 2017; Chen & Friedman, 2017; Gao et al., 2018; Ghoshdastidar et al., 2017; Ghoshdastidar & von Luxburg, 2018; Li & Wang, 2018; Kirchler et al., 2020). These tests have also allowed application in various machine learning problems such as domain adaptation, generative modeling, and causal discovery (Binkowski et al., 2018; Gong et al., 2016; Stojanov et al., 2019; Lopez-Paz & Oquab, 2017).

A popular class of non-parametric two-sample tests is based on kernel methods (Smola & Schölkopf, 2001): such tests construct a *kernel mean embedding* (Berlinet & Thomas-Agnan, 2004; Muandet et al., 2017) for each distribution, and measure the difference in these embeddings. For any *characteristic* kernel, two distributions are the same if and only if their mean embeddings are the same; the distance between mean embeddings is the *maximum mean discrepancy* (MMD) (Gretton et al., 2012a). There are also several closely related methods, including tests based on checking for differences in mean embeddings evaluated at specific locations (Chwialkowski et al., 2015; Jitkrittum et al., 2016) and kernel Fisher discriminant analysis (Harchaoui et al., 2007). These tests all work well for samples from simple distributions when using appropriate kernels.

Problems that we care about, however, often involve distributions with complex structure, where simple kernels will often map distinct distributions to nearby (and hence hard to distinguish) mean embeddings. Figure 1a shows an example of a multimodal dataset, where the overall modes align but the sub-mode structure varies differently at each mode. A translation-invariant Gaussian kernel only “looks at” the data uniformly within each mode (see Figure 1b), requiring many samples to correctly distinguish the two distributions. The distributions can be distinguished more effectively if we understand the structure of each mode, as with the more complex kernel illustrated in Figure 1c.

To model these complex functions, we adopt a *deep kernel* approach (Wilson et al., 2016; Sutherland et al., 2017; Li et al., 2017; Jean et al., 2018; Wenliang et al., 2019),

^{*}Equal contribution ¹Australian Artificial Intelligence Institute, University of Technology Sydney, Sydney, NSW, Australia ²Gatsby Computational Neuroscience Unit, University College London, London, UK ³Toyota Technological Institute at Chicago, Chicago, IL, USA. Correspondence to: Feng Liu <Feng.Liu@uts.edu.au>, Wenkai Xu <wenkaix@gatsby.ucl.ac.uk>, D.J. Sutherland <djs@djsutherland.ml>.

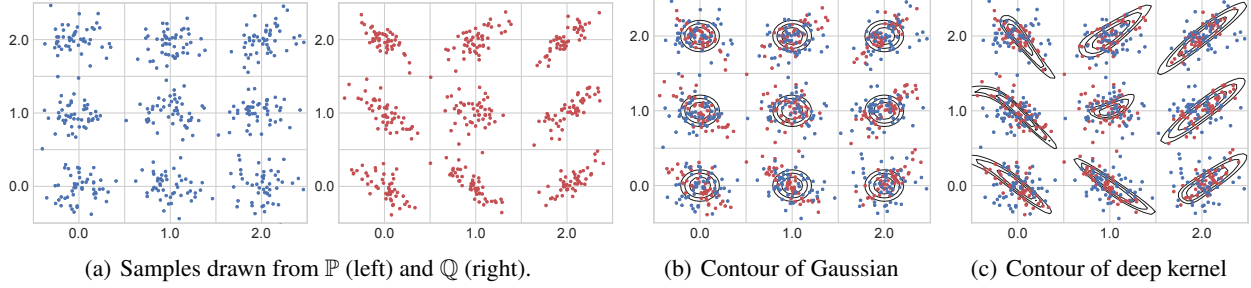


Figure 1. In the Blob dataset, \mathbb{P} and \mathbb{Q} are each equal mixtures of nine Gaussians with the same modes (a), but each component of \mathbb{P} is an isotropic Gaussian whereas the covariance of \mathbb{Q} differs in each component. Panels (b) and (c) show the contours of a kernel, $k(x, \mu_i)$ for each of the nine modes μ_i ; contour values are 0.7, 0.8 and 0.9. A Gaussian kernel (b) treats points isotropically throughout the space, based only on $\|x - y\|$. A deep kernel (c) learned by our methods behaves differently in different parts of the space, adapting to the local structure of the data distributions and hence allowing better identification of differences between \mathbb{P} and \mathbb{Q} .

building a kernel with a deep network. In this paper, we use

$$k_\omega(x, y) = [(1 - \epsilon)\kappa(\phi_\omega(x), \phi_\omega(y)) + \epsilon]q(x, y), \quad (1)$$

where the deep neural network ϕ_ω extracts features of samples, and κ is a simple kernel (e.g., a Gaussian) on those features, while q is a simple characteristic kernel (e.g. Gaussian) on the input space. With an appropriate choice of ϕ_ω , this allows for extremely flexible kernels which can learn complex behavior very different in different parts of space. This choice is discussed further in Section 5.

These complex kernels, though, cannot feasibly be specified by hand or simple heuristics, as is typical practice in kernel methods. We select the parameters ω by maximizing the ratio of the MMD to its variance, which maximizes test power at large sample sizes. This procedure was proposed by Sutherland et al. (2017), but we establish for the first time that it gives consistent selection of the best kernel in the class, whether optimizing our deep kernels with hundreds of thousands of parameters or simply choosing lengthscales of a Gaussian as did Sutherland et al. Previously, there were no guarantees this procedure would yield a kernel which generalized at all from the training set to a test set.

Another way to compare distributions is to train a classifier between them, and evaluate its accuracy (Lopez-Paz & Oquab, 2017). We show, perhaps surprisingly, that our framework encompasses this approach, but deep kernels allow for more general model classes which can use the data more efficiently. We also train representations directly to maximize test power, rather than a cross-entropy surrogate.

We test our method on several simulated and real-world datasets, including complex synthetic distributions, high-energy physics data, and challenging image problems. We find convincingly that learned deep kernels outperform simple shallow methods, and learning by maximizing test power outperforms learning through a cross-entropy surrogate loss.

2. MMD Two-Sample Tests

Two-sample testing. Let \mathcal{X} be a separable metric space – in this paper, typically a subset of \mathbb{R}^d – and \mathbb{P}, \mathbb{Q} be Borel probability measures on \mathcal{X} . We observe independent identically distributed (*i.i.d.*) samples $S_\mathbb{P} = \{x_i\}_{i=1}^n \sim \mathbb{P}^n$ and $S_\mathbb{Q} = \{y_j\}_{j=1}^m \sim \mathbb{Q}^m$. We wish to know whether $S_\mathbb{P}$ and $S_\mathbb{Q}$ come from the same distribution: does $\mathbb{P} = \mathbb{Q}$?

We use the null hypothesis testing framework, where the null hypothesis $\mathfrak{H}_0 : \mathbb{P} = \mathbb{Q}$ is tested against the alternative hypothesis $\mathfrak{H}_1 : \mathbb{P} \neq \mathbb{Q}$. We perform a two-sample test in four steps: select a significance level $\alpha \in [0, 1]$; compute a test statistic $\hat{t}(S_\mathbb{P}, S_\mathbb{Q})$; compute the p -value $\hat{p} = \Pr_{\mathfrak{H}_0}(T > \hat{t})$, the probability of the two-sample test returning a statistic as large as \hat{t} when \mathfrak{H}_0 is true; finally, reject \mathfrak{H}_0 if $\hat{p} < \alpha$.

Maximum mean discrepancy (MMD). We will base our two-sample test statistic on an estimate of a distance between distributions. Our metric, the MMD, is defined in terms of a kernel k giving point-level “similarities” on \mathcal{X} .

Definition 1 (Gretton et al., 2012a). *Let $k : \mathcal{X} \times \mathcal{X} \rightarrow \mathbb{R}$ be the kernel of a reproducing kernel Hilbert space \mathcal{H}_k , with feature maps $k(\cdot, x) \in \mathcal{H}_k$. Let $X, X' \sim \mathbb{P}$ and $Y, Y' \sim \mathbb{Q}$, and define the kernel mean embeddings $\mu_\mathbb{P} := \mathbb{E}[k(\cdot, X)]$ and $\mu_\mathbb{Q} := \mathbb{E}[k(\cdot, Y)]$. Under mild integrability conditions,*

$$\begin{aligned} \text{MMD}(\mathbb{P}, \mathbb{Q}; \mathcal{H}_k) &:= \sup_{f \in \mathcal{H}_k, \|f\|_{\mathcal{H}_k} \leq 1} |\mathbb{E}[f(X)] - \mathbb{E}[f(Y)]| \\ &= \|\mu_\mathbb{P} - \mu_\mathbb{Q}\|_{\mathcal{H}_k} = \sqrt{\mathbb{E}[k(X, X') + k(Y, Y') - 2k(X, Y)]}. \end{aligned}$$

For characteristic kernels, $\mu_\mathbb{P} = \mu_\mathbb{Q}$ implies $\mathbb{P} = \mathbb{Q}$, hence $\text{MMD}(\mathbb{P}, \mathbb{Q}; \mathcal{H}_k) = 0$ if and only if $\mathbb{P} = \mathbb{Q}$.

The first form shows that the MMD is an integral probability metric (Müller, 1997), along with such popular distances as the Wasserstein and total variation.

There are several natural estimators of the MMD from samples. We will assume $n = m$ and use the U -statistic estima-

tor, which is unbiased for MMD^2 and has nearly minimal variance among unbiased estimators (Gretton et al., 2012a):

$$\widehat{\text{MMD}}_u^2(S_{\mathbb{P}}, S_{\mathbb{Q}}; k) := \frac{1}{n(n-1)} \sum_{i \neq j} H_{ij} \quad (2)$$

$$H_{ij} := k(X_i, X_j) + k(Y_i, Y_j) - k(X_i, Y_j) - k(Y_i, X_j).$$

The similar $\widehat{\text{MMD}}_b^2 := \frac{1}{n^2} \sum_{i,j} H_{ij}$ is the squared MMD between the empirical distributions of $S_{\mathbb{P}}$ and $S_{\mathbb{Q}}$.¹

Testing with the MMD. It can be shown that under \mathfrak{H}_0 , $n\widehat{\text{MMD}}_u^2$ converges to a distribution depending on \mathbb{P} and k ; we thus use this as our test statistic.

Proposition 2 (Asymptotics of $\widehat{\text{MMD}}_u^2$). *Under the null hypothesis, $\mathfrak{H}_0 : \mathbb{P} = \mathbb{Q}$, we have if $Z_i \sim \mathcal{N}(0, 2)$,*

$$n\widehat{\text{MMD}}_u^2 \xrightarrow{d} \sum_i \sigma_i (Z_i^2 - 2);$$

here σ_i are the eigenvalues of the \mathbb{P} -covariance operator of the centered kernel (Gretton et al., 2012a, Theorem 12), and \xrightarrow{d} denotes convergence in distribution.

Under the alternative, $\mathfrak{H}_1 : \mathbb{P} \neq \mathbb{Q}$, a standard central limit theorem holds (Serfling, 1980, Section 5.5.1):

$$\begin{aligned} \sqrt{n}(\widehat{\text{MMD}}_u^2 - \text{MMD}^2) &\xrightarrow{d} \mathcal{N}(0, \sigma_{\mathfrak{H}_1}^2) \\ \sigma_{\mathfrak{H}_1}^2 &:= 4 \left(\mathbb{E}[H_{12}H_{13}] - \mathbb{E}[H_{12}]^2 \right) \end{aligned}$$

where H_{12}, H_{13} refer to H_{ij} above.

Although it is possible to construct a test based on directly estimating this null distribution (Gretton et al., 2009), it is both simpler and, if implemented carefully, faster (Sutherland et al., 2017) to instead use a permutation test. This general method (Dwass, 1957; Alba Fernández et al., 2008) observes that under \mathfrak{H}_0 , the samples from \mathbb{P} and \mathbb{Q} are interchangeable; we can therefore estimate the null distribution of our test statistic by repeatedly re-computing it with the samples randomly re-assigned to $S_{\mathbb{P}}$ or $S_{\mathbb{Q}}$.

Test power. The main measure of efficacy of a null hypothesis test is its *power*: the probability that, for a particular $\mathbb{P} \neq \mathbb{Q}$ and n , we correctly reject \mathfrak{H}_0 . Proposition 2 implies, where Φ is the standard normal CDF, that

$$\Pr_{\mathfrak{H}_1} \left(n\widehat{\text{MMD}}_u^2 > r \right) \rightarrow \Phi \left(\frac{\sqrt{n} \text{MMD}^2}{\sigma_{\mathfrak{H}_1}} - \frac{r}{\sqrt{n} \sigma_{\mathfrak{H}_1}} \right);$$

¹Including $k(X_i, Y_i)$ terms in $\widehat{\text{MMD}}_u^2$ gives the minimal variance unbiased estimator, and allows $m \neq n$. The U -statistic is more convenient for analysis and for efficient permutations; in our settings it behaves similarly to the MVUE and $\widehat{\text{MMD}}_b^2$.

we can find the approximate test power by using the rejection threshold, found via (e.g.) permutation testing, as r . We also know via Proposition 2 that this r will converge to a constant, and MMD , $\sigma_{\mathfrak{H}_1}$ are also constants. For reasonably large n , the power is dominated by the first term, and the kernel yielding the most powerful test will approximately maximize (Sutherland et al., 2017)

$$J(\mathbb{P}, \mathbb{Q}; k) := \text{MMD}^2(\mathbb{P}, \mathbb{Q}; k) / \sigma_{\mathfrak{H}_1}(\mathbb{P}, \mathbb{Q}; k). \quad (3)$$

Selecting a kernel. The criterion $J(\mathbb{P}, \mathbb{Q}; k)$ depends on the particular \mathbb{P} and \mathbb{Q} at hand, and thus we typically will neither be able to choose a kernel *a priori*, nor exactly evaluate J given samples. We can, however, estimate it with

$$\hat{J}_{\lambda}(S_{\mathbb{P}}, S_{\mathbb{Q}}; k) := \frac{\widehat{\text{MMD}}_u^2(S_{\mathbb{P}}, S_{\mathbb{Q}}; k)}{\hat{\sigma}_{\mathfrak{H}_1, \lambda}^2(S_{\mathbb{P}}, S_{\mathbb{Q}}; k)}, \quad (4)$$

where $\hat{\sigma}_{\mathfrak{H}_1, \lambda}^2$ is a regularized estimator of $\sigma_{\mathfrak{H}_1}^2$ given by²

$$\frac{4}{n^3} \sum_{i=1}^n \left(\sum_{j=1}^n H_{ij} \right)^2 - \frac{4}{n^4} \left(\sum_{i=1}^n \sum_{j=1}^n H_{ij} \right)^2 + \lambda. \quad (5)$$

Given $S_{\mathbb{P}}$ and $S_{\mathbb{Q}}$, we could construct a test by choosing k to maximize $\hat{J}_{\lambda}(S_{\mathbb{P}}, S_{\mathbb{Q}}; k)$, then using a test statistic based on $\widehat{\text{MMD}}(S_{\mathbb{P}}, S_{\mathbb{Q}}; k)$. This sample re-use, however, violates the conditions of Proposition 2, and permutation testing would require repeatedly re-training k with permuted labels.

Thus we split the data, get $k^{tr} \approx \arg \max_k \hat{J}_{\lambda}(S_{\mathbb{P}}^{tr}, S_{\mathbb{Q}}^{tr}; k)$, then compute the test statistic and permutation threshold on $S_{\mathbb{P}}^{te}, S_{\mathbb{Q}}^{te}$ using k^{tr} . This procedure was proposed for $\widehat{\text{MMD}}_u^2$ by Sutherland et al. (2017), but the same technique works for a variety of tests (Gretton et al., 2012b; Jitkrittum et al., 2016; 2017; Lopez-Paz & Oquab, 2017). Our paper adopts this framework (Section 5) and studies it further.

Relationship to other approaches. One common scheme is to pick a kernel k_{ω} based on some proxy task, such as a related classification problem (e.g. Kirchler et al. 2020 or the KID score of Binkowski et al. 2018). Although this approach can work quite well, it depends entirely on features from the proxy task applying well to the differences between \mathbb{P} and \mathbb{Q} , which can be hard to know in general.

An alternative is to maximize simply $\widehat{\text{MMD}}_u$ (Sriperumbudur et al. 2009; proposed but not evaluated by Kirchler

²This estimator, as a V -statistic, is biased even when $\lambda = 0$ (although this bias is only $O(1/N)$; see Lemma 18). Although Sutherland et al. (2017); Sutherland (2019) give a quadratic-time estimator unbiased for $\sigma_{\mathfrak{H}_1}^2$, it is much more complicated to implement and analyze, likely has higher variance, and (being unbiased) can be negative, especially e.g. when the kernel is poor.

et al.). Ignoring $\sigma_{\mathcal{S}_1}$ means that, for instance, this approach would choose to simply scale $k \rightarrow \infty$, even though this does not change the test at all. Even when this is not possible, Sutherland et al. (2017) found this approach notably worse than maximizing (4); we confirm this in our experiments.

MMD-GANs (Li et al., 2017; Binkowski et al., 2018) also simply maximize $\widehat{\text{MMD}}_u$ to identify the differences between their model \mathbb{Q}_θ and target \mathbb{P} . If \mathbb{Q}_θ is quite far from \mathbb{P} , however, an MMD-GAN requires a “weak” kernel to identify a path for improving \mathbb{Q}_θ (Arbel et al., 2018), while our ideal kernel is one which perfectly distinguishes \mathbb{P} and \mathbb{Q}_θ and would likely give no signal for improvement. Our algorithm, theoretical guarantees, and empirical evaluations thus all differ significantly from those for MMD-GANs.

3. Limits of Simple Kernels

We can use the criterion \hat{J}_λ of (4) even to select parameters among a simple family, such as the lengthscale of a Gaussian kernel. Doing so on the *Blob* problem of Figure 1 illustrates the limitations of using MMD with these kernels.

In Figure 2c, we show how the maximal value of \hat{J} changes as we see more samples from \mathbb{P} and \mathbb{Q} , for both a family of Gaussian kernels (green dashed line) and a family (1) of deep kernels (red line). The optimal \hat{J} is always higher for the deep kernels; as expected, the empirical test power (Figure 2a) is also higher for deep kernels.

Most simple kernels used for MMD tests, whether the Gaussian we use here or Laplace, inverse multiquadric, even automatic relevance determination kernels, are all translation invariant: $k(x, y) = k(x - t, y - t)$ for any $t \in \mathbb{R}^d$. (All kernels used by Sutherland et al. (2017), for instance, were of this type.) Hence the kernel behaves the same way across space, as in Figure 1b. This means that for distributions whose behavior varies through space, whether because principal directions change (as in Figure 1) so the shape should be different, or because some regions are much denser than others and so need a smaller lengthscale (e.g. Wenliang et al., 2019, Figures 1 and 2), any single global choice is suboptimal.

Kernels which are not translation invariant, such as the deep kernels (1) shown in Figure 1c, can adapt to the different shapes necessary in different areas.

4. Relationship to Classifier-Based Tests

Another popular method for conducting two-sample tests is to train a classifier between $S_\mathbb{P}^{tr}$ and $S_\mathbb{Q}^{tr}$, then assess its performance on $S_\mathbb{P}^{te}$, $S_\mathbb{Q}^{te}$. If $\mathbb{P} = \mathbb{Q}$, the classification problem is impossible and performance will be at chance.

The most common performance metric is the accuracy

(Lopez-Paz & Oquab, 2017); this scheme is fairly common among practitioners, and Kim et al. (2020) showed it to be optimal in rate, but suboptimal in constant, in one limited setting (linear discriminant analysis between high-dimensional elliptical distributions, e.g. Gaussians, with identical covariances). We will call this approach a Classifier Two-Sample Test based on Sign, C2ST-S. Letting $f : \mathcal{X} \rightarrow \mathbb{R}$ output classification scores, the C2ST-S statistic is $\widehat{\text{acc}}(S_\mathbb{P}, S_\mathbb{Q}; f)$ given by

$$\frac{1}{2n} \sum_{X_i \in S_\mathbb{P}} \mathbb{1}(f(X_i) > 0) + \frac{1}{2n} \sum_{Y_i \in S_\mathbb{Q}} \mathbb{1}(f(Y_i) \leq 0).$$

Let $\text{acc}(\mathbb{P}, \mathbb{Q}; f) := \frac{1}{2} \Pr(f(X) > 0) + \frac{1}{2} \Pr(f(Y) \leq 0)$; $\widehat{\text{acc}}$ is unbiased for acc and has a simple asymptotically normal null distribution.

Although it is perhaps not immediately obvious this is the case, C2ST-S is almost a special case of the MMD. Let

$$k_f^{(S)}(x, y) = \frac{1}{4} \mathbb{1}(f(x) > 0) \mathbb{1}(f(y) > 0). \quad (6)$$

A C2ST-S with f is equivalent to an MMD test with $k_f^{(S)}$:

Proposition 3. *It holds that*

$$\begin{aligned} \text{MMD}(\mathbb{P}, \mathbb{Q}; k_f^{(S)}) &= |\text{acc}(\mathbb{P}, \mathbb{Q}; f) - \frac{1}{2}| \\ \widehat{\text{MMD}}_b(S_\mathbb{P}, S_\mathbb{Q}; k_f^{(S)}) &= |\widehat{\text{acc}}(S_\mathbb{P}, S_\mathbb{Q}; f) - \frac{1}{2}|. \end{aligned}$$

Proof. The mean embedding $\mu_\mathbb{P}$ under $k_f^{(S)}$ is simply $\frac{1}{2} \mathbb{E} \mathbb{1}(f(X) > 0) = \frac{1}{2} \Pr(f(X) > 0)$, so the MMD is

$$\frac{1}{2} \left| \Pr(f(X) > 0) - \Pr(f(Y) > 0) \right| = \left| \text{acc}(\mathbb{P}, \mathbb{Q}; f) - \frac{1}{2} \right|.$$

Moreover, $\widehat{\text{acc}}$ is acc on empirical distributions. \square

The C2ST-S, however, selects f to maximize cross-entropy (approximately maximizing $\widehat{\text{acc}}$), while we maximize \hat{J}_λ (4). Although $k_f^{(S)}$ is not differentiable, maximizing (3) would exactly maximize acc and hence maximize test power (Lopez-Paz & Oquab, 2017, Theorem 1).

Accessing f only through its sign allows for a simple null distribution, but it ignores f ’s measure of confidence: a highly confident output extremely far from the decision boundary is treated the same as a very uncertain one lying in an area of high overlap between \mathbb{P} and \mathbb{Q} , dramatically increasing the variance of the statistic. A scheme we call C2ST-L instead tests difference in means of f on \mathbb{P} and \mathbb{Q} (Chen & Cloninger, 2019). Let

$$k_f^{(L)}(x, y) = f(x)f(y). \quad (7)$$

A C2ST-L is equivalent to an MMD test with $k_f^{(L)}$:

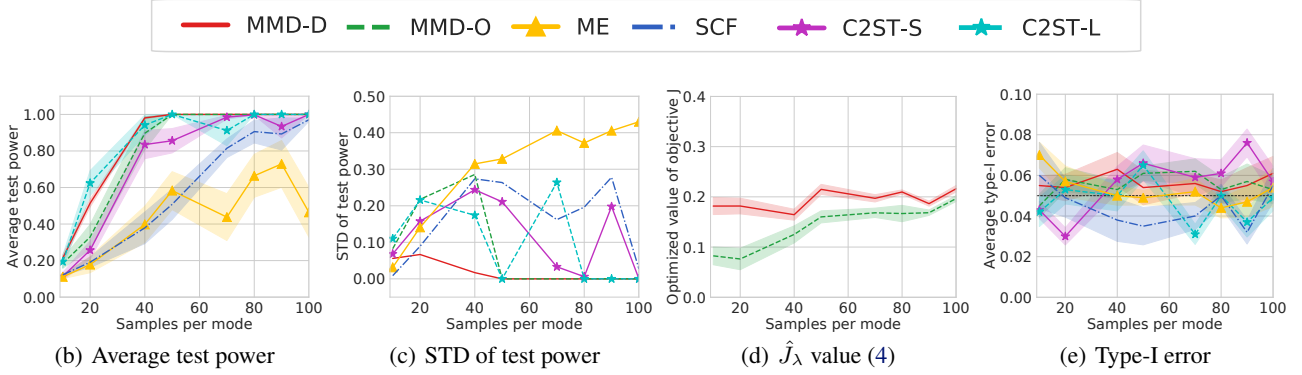


Figure 2. Results on *Blob-S* and *Blob-D* given $\alpha = 0.05$; see Section 7 for details. n_b is the number of samples at each mode, so $n_b = 100$ means drawing 900 samples from each of \mathbb{P} and \mathbb{Q} . We report, when increasing n_b , (a) average test power, (b) standard deviation of test power, (c) the value of \hat{J}_λ , and (d) average type-I error. (a), (b) and (c) are on *Blob-D*, and (d) is on *Blob-S*. Shaded regions show standard errors for the mean, and the black line shows α .

Proposition 4. *It holds that*

$$\begin{aligned} \text{MMD}(\mathbb{P}, \mathbb{Q}; k_f^{(L)}) &= |\mathbb{E} f(X) - \mathbb{E} f(Y)| \\ \widehat{\text{MMD}}_b(S_{\mathbb{P}}, S_{\mathbb{Q}}; k_f^{(L)}) &= \left| \frac{1}{n} \sum_{X_i \in S_{\mathbb{P}}} f(X_i) - \frac{1}{n} \sum_{Y_i \in S_{\mathbb{Q}}} f(Y_i) \right|. \end{aligned}$$

Proof. This kernel’s feature map is $k_f^{(L)}(x, \cdot) = f(x)$. \square

Now maximizing accuracy (or a cross-entropy proxy) no longer directly maximizes power. This kernel is differentiable, so we can directly compare the merits of maximizing (4) to maximizing cross-entropy; we will see in Section 7.2 that our more direct approach is empirically superior.

Compared to using $k_f^{(L)}$, however, Section 7.2 shows that learned MMD tests also obtain better performance using kernels like (1). This is analogous to a similar phenomenon observed in other problems by Binkowski et al. (2018) and Wenliang et al. (2019): C2STs learn a full discriminator function on the training set, and then apply only that function to the test set. Learning a deep kernel like (1) corresponds to learning only a powerful *representation* on the training set, and then *still learning* f itself from the test set – in a closed form that makes permutation testing simple.

5. Learning Deep Kernels

Choice of kernel architecture. Most previous work on deep kernels has used a kernel κ directly on the output of a featurization network ϕ_ω , $k_\omega(x, y) = \kappa(\phi_\omega(x), \phi_\omega(y))$. This is certainly also an option for us. Any such k_ω , however, is characteristic if and only if ϕ_ω is injective. If we select our kernel well, this is not really a concern.³ Even so, it

³A characteristic kernel on top of even $\phi_\omega(x) = \omega^\top x$ with a *random* ω will be almost surely consistent (Heller & Heller, 2016), and in general the existence of even one good ϕ_ω for a particular

would be reassuring to know that, even if the optimization goes awry, the resulting test will still be at least consistent. More importantly, it can be helpful in optimization to add a “safeguard” preventing the learned kernel from considering extremely far-away inputs as too similar. We can achieve these goals with the form (1), repeated here:

$$k_\omega(x, y) = [(1 - \epsilon)\kappa(\phi_\omega(x), \phi_\omega(y)) + \epsilon] q(x, y).$$

Here ϕ_ω is a deep network (with parameters ω) that extracts features, and κ is a kernel on those features; we use a Gaussian with lengthscale σ_ϕ , $\kappa(a, b) = \exp\left(-\frac{1}{2\sigma_\phi^2}\|a - b\|^2\right)$. We choose $0 < \epsilon < 1$ and q a Gaussian with lengthscale σ_q .

Proposition 5. *Let k_ω be of the form (1) with $\epsilon > 0$ and q characteristic. Then k_ω is characteristic.*

Learning the deep kernel. The kernel optimization and testing procedure is summarized in Algorithm 1. For larger datasets, or when $n \neq m$, we use minibatches in the training procedure; for smaller datasets, we use full batches. We use the Adam optimizer (Kingma & Ba, 2015). Note that the parameters ϵ , σ_ϕ , and σ_q are included in ω , all parameterized in log-space (i.e. we optimize ϵ' where $\epsilon = \exp(\epsilon')$).

Time complexity. Let E denote the cost of computing an embedding $\phi_\omega(x)$, and K the cost of computing (1) given $\phi_\omega(x)$, $\phi_\omega(y)$. Then each iteration of training in Algorithm 1 costs $\mathcal{O}(mE + m^2K)$, where m is the minibatch size; for the moderate m that fit in a GPU-sized minibatch anyway, the mE term typically dominates, matching the complexity of a C2ST. Testing takes time $\mathcal{O}(nE + n^2K + n^2n_{\text{perm}})$, compared to $\mathcal{O}(nE + nn_{\text{perm}})$ for permutation-based C2STs. In either case, the quadratic factors could if necessary be reduced

\mathbb{P} , \mathbb{Q} pair is enough that a perfect optimizer would be able to distinguish the distributions (Arbel et al., 2018, Proposition 1).

Algorithm 1 Testing with a learned deep kernel

Input: S_P, S_Q , various hyperparameters used below;
 $\omega \leftarrow \omega_0; \lambda \leftarrow 10^{-8};$
 Split the data as $S_P = S_P^{tr} \cup S_P^{te}$ and $S_Q = S_Q^{tr} \cup S_Q^{te};$
Phase 1: train the kernel parameters ω on S_P^{tr} and S_Q^{tr}
for $T = 1, 2, \dots, T_{max}$ **do**
 $X \leftarrow \text{minibatch from } S_P^{tr}; Y \leftarrow \text{minibatch from } S_Q^{tr};$
 $k_\omega \leftarrow \text{kernel function with parameters } \omega; \quad \# \text{ as in (1)}$
 $M(\omega) \leftarrow \widehat{\text{MMD}}_u^2(X, Y; k_\omega); \quad \# \text{ using (2)}$
 $V_\lambda(\omega) \leftarrow \hat{\sigma}_{\mathfrak{H}_1, \lambda}^2(X, Y; k_\omega); \quad \# \text{ using (5)}$
 $\hat{J}_\lambda(\omega) \leftarrow M(\omega) / \sqrt{V_\lambda(\omega)}; \quad \# \text{ as in (4)}$
 $\omega \leftarrow \omega + \eta \nabla_{\text{Adam}} \hat{J}_\lambda(\omega); \quad \# \text{ maximize } \hat{J}_\lambda(\omega)$
end for
Phase 2: permutation test with k_ω on S_P^{te} and S_Q^{te}
 $est \leftarrow \widehat{\text{MMD}}_u^2(S_P^{te}, S_Q^{te}; k_\omega)$
for $i = 1, 2, \dots, n_{perm}$ **do**
 Shuffle $S_P^{te} \cup S_Q^{te}$ into X and Y
 $perm_i \leftarrow \widehat{\text{MMD}}_u^2(X, Y; k_\omega)$
end for
Output: $k_\omega, est, p\text{-value } \frac{1}{n_{perm}} \sum_{i=1}^{n_{perm}} \mathbb{1}(perm_i \geq est)$

with the block estimator approach of Zaremba et al. (2013), at the cost of some test power. In our experiments in Section 7, the overall runtime of our methods was scarcely different from the overall runtime of C2STs.

6. Theoretical Analysis

We now show that optimizing the regularized test power criterion based on a finite number of samples works: as n increases, our estimates converge uniformly over a ball in parameter space, and therefore if there is a unique best kernel, we converge to it. Sutherland et al. (2017) gave no such guarantees; this result allows us to trust that, at least for reasonably large n and if our optimization process succeeds, we will find a kernel that generalizes nearly optimally rather than just overfitting to S^{tr} .

We first state a generic result, then show some choices of kernels, particularly deep kernels (1), satisfy the conditions.

Theorem 6. *Let ω parameterize uniformly bounded kernel functions k_ω in a Banach space of dimension D , with $|k_\omega(x, y) - k_{\omega'}(x, y)| \leq L_k \|\omega - \omega'\|$. Let $\bar{\Omega}_s$ be a set of ω for which $\sigma_{\mathfrak{H}_1}^2(\mathbb{P}, \mathbb{Q}; k_\omega) \geq s^2 > 0$ and $\|\omega\| \leq R_\Omega$. Take $\lambda = n^{-1/3}$. Then, with probability at least $1 - \delta$,*

$$\sup_{\omega \in \bar{\Omega}_s} |\hat{J}_\lambda(S_P, S_Q; k_\omega) - J(\mathbb{P}, \mathbb{Q}; k_\omega)| = \mathcal{O} \left(\frac{1}{s^2 n^{1/3}} \left[\frac{1}{s} + \sqrt{D \log(R_\Omega n) + \log \frac{1}{\delta}} + L_k \right] \right).$$

If there is a unique best kernel ω^ , the maximizer of \hat{J}_λ converges in probability to ω^* as $n \rightarrow \infty$.*

A version with explicit constants and more details is given in Appendix A (as Theorem 11 and Corollary 12); the proof is based on uniform convergence of the MMD and variance estimators using an ϵ -net argument.

The following results are shown in Appendix A.4. We first show a result on simple Gaussian bandwidth selection.

Proposition 7. *Suppose each $x \in \mathcal{X}$ has $\|x\| \leq R_X$, and we choose the bandwidth of a Gaussian kernel among a set whose minimum is at least $1/R_\Omega$. Then the conditions of Theorem 6 are met with $D = 1$ and $L_k = 2R_X/\sqrt{e}$.*

Our results also apply to multiple kernel learning, where in fact the exact maximizer of \hat{J}_λ is efficiently available (Proposition 27).

Proposition 8. *Let $\{k_i\}_{i=1}^D$ be a fixed set of kernels, with $\sup_x k_i(x, x) \leq K$ for all i . Then picking $k_\omega = \sum_{i=1}^D \omega_i k_i$ among some set of ω with $\sum_{i=1}^D \omega_i^2 \leq R_\Omega^2$ satisfies the conditions of Theorem 6 with $L_k = K\sqrt{D}$.*

We finally establish our results for fully-connected deep kernels; it also applies to convolutional networks with a slightly different R_Ω (Remark 25). The constants in L_k are given in Proposition 23.

Proposition 9. *Take k_ω as in Section 5, with ϕ_ω a fully-connected network with depth Λ and D total parameters, whose activations are 1-Lipschitz with $\sigma(0) = 0$ (e.g. ReLU). Suppose the operator norm of each weight matrix and L_2 norm of each bias vector are at most R_Ω , and each $x \in \mathcal{X}$ has $\|x\| \leq R_X$. Then k_ω meets the conditions of Theorem 6 with dimension D and $L_K = \mathcal{O} \left(\Lambda R_\Omega^{\Lambda-1} \frac{R_X+1}{\sigma_\phi} \right)$.*

The dependence on s in Theorem 6 is somewhat unfortunate, but the ratio structure of J means that otherwise, errors in very small variances can hurt us arbitrarily. Even so, “near-perfect” kernels (with reasonably large MMD and very small variance) will likely still be chosen as the maximizer of the regularized criterion, even if we do not estimate the (extremely large) ratio accurately. Likewise, near-constant kernels (with very small variance but still small J) will generally have their J underestimated, and so are unlikely to be selected when a better kernel is available. The ϵq component in (1) may also help avoid extremely small variances.

Given N data points, this result also gives insight into how many we should use to train the kernel and how many to test. With perfect optimization, Corollary 14 shows a bound on the asymptotic power of the test is maximized by training on $\Theta \left((N\sqrt{\log N})^{\frac{3}{4}} \right)$ points, and testing on the remainder.

7. Experimental Results

7.1. Comparison on Benchmark Datasets

We compare the following tests on several datasets:

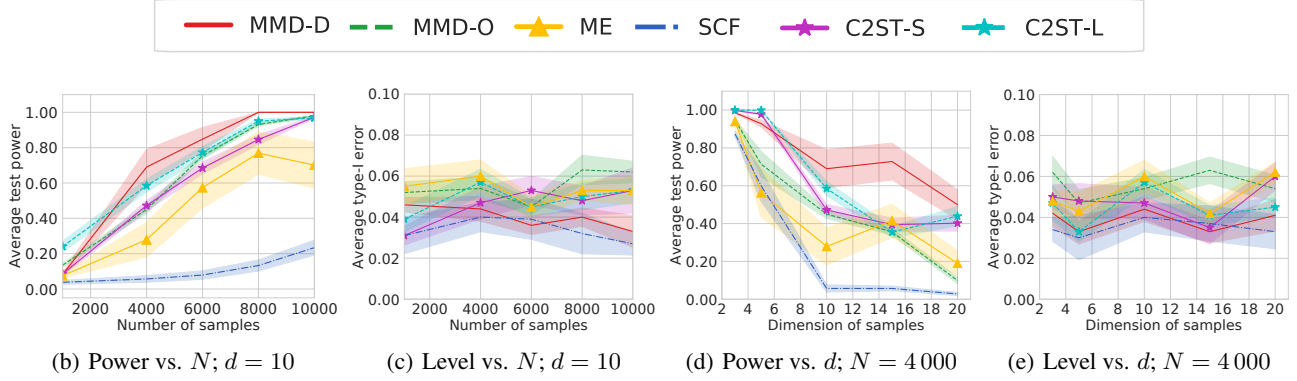


Figure 3. Results on *HDGM-S* and *HDGM-D* for $\alpha = 0.05$ (black line). Left: average test power (a) and Type I error (b) when increasing the number of samples N , keeping $d = 10$. Right: average test power (c) and Type I error (d) when increasing the dimension d , keeping $N = 4000$. Shaded regions show standard errors for the mean.

- **MMD-D**: MMD with a deep kernel; our method described in Section 5.
- **MMD-O**: MMD with a Gaussian kernel whose length-scale is optimized as in Section 5. This gives better results than standard heuristics.
- **Mean embedding (ME)**: a state-of-the-art test (Chwialkowski et al., 2015; Jitkrittum et al., 2016) based on differences in Gaussian kernel mean embeddings at a set of optimized points.
- **Smooth characteristic functions (SCF)**: a state-of-the-art test (Chwialkowski et al., 2015; Jitkrittum et al., 2016) based on differences in Gaussian mean embeddings at a set of optimized frequencies.
- **Classifier two-sample tests**, including C2STS-S (Lopez-Paz & Oquab, 2017) and C2ST-L (Chen & Cloninger, 2019) as described in Section 4. We set the test thresholds via permutation for both.

For synthetic datasets, we take a single sample set for $S_{\mathbb{P}}^{tr}$ and $S_{\mathbb{Q}}^{tr}$ and learn a kernel/test locations/etc once for each method on that training set. We then evaluate its rejection rate on 100 new sample sets $S_{\mathbb{P}}^{te}$, $S_{\mathbb{Q}}^{te}$ from the same distribution. For real datasets, we select a subset of the available data for $S_{\mathbb{P}}^{tr}$ and $S_{\mathbb{Q}}^{tr}$ and train on that; we then evaluate on 100 random subsets, disjoint from the training set, of the remaining data. We repeat this full process 10 times, and report the mean rejection rate of each test. Table 5 shows significance tests. Further details are in Appendix B.

Blob dataset. *Blob-D* is the dataset shown in Figure 1; *Blob-S* has \mathbb{Q} also equal to the distribution shown in Figure 1a, so that the null hypothesis holds. Details are given in Table 6 (Appendix B.1).

Results are shown in Figure 2. MMD-D and C2ST-L are the clear winners in power, with MMD-D better in the higher-sample regime, and MMD-D is more reliable than C2STs. Figure 2c shows that J is higher for MMD-D than MMD-O,

in addition to the actual test power being better, as discussed in Section 3. All methods have expected Type I error rates.

High-dimensional Gaussian mixtures. Here we study bimodal Gaussian mixtures in increasing dimension. Each distribution has two Gaussian components; in *HDGM-S*, \mathbb{P} and \mathbb{Q} are the same, while in *HDGM-D*, \mathbb{P} and \mathbb{Q} differ in the covariance of a single dimension pair but are otherwise the same. Details are in Table 6 (Appendix B.1). We consider both increasing N while keeping $d = 10$ and increasing d while keeping $N = 4000$, with results shown in Figure 3. Again, MMD-D has generally the best test power across a range of problem settings, with reasonable type I error.

Higgs dataset (Baldi et al., 2014). We compare the jet ϕ -momenta distribution ($d = 4$) of the background process, \mathbb{P} , which lacks Higgs bosons, to the corresponding distribution \mathbb{Q} for the process that produces Higgs bosons, following Chwialkowski et al. (2015). As discussed in these previous works, ϕ -momenta carry very little discriminating information for recognizing whether Higgs bosons were produced. We consider a series of tests with increased number of samples N .

We report average test power (comparing \mathbb{P} to \mathbb{Q}) in Table 1, and average type-I error (comparing \mathbb{P} to \mathbb{P} or \mathbb{Q} to \mathbb{Q}) in Table 7 (Appendix B.6). As before, MMD-D generally performs the best; although the improvement over MMD-O here is not dramatic, MMD-D does notably outperform C2ST. All methods maintain reasonable Type I errors.

MNIST generative model. The *MNIST* dataset contains 70 000 handwritten digit images (LeCun et al., 1998). We compare true *MNIST* data samples \mathbb{P} to samples \mathbb{Q} from a pretrained deep convolutional generative adversarial network (DCGAN) (Radford et al., 2016). Samples from both distributions are shown in Figure 4 (in Appendix B.2).

We consider tests for increasing numbers of samples N , and report average test power (for \mathbb{P} to \mathbb{Q}) in Table 2 and

Table 1. *Higgs* ($\alpha = 0.05$): average test power \pm standard error for N samples. Bold represents the highest mean per row.

N	ME	SCF	C2ST-S	C2ST-L	MMD-O	MMD-D
1 000	0.120 \pm 0.007	0.095 \pm 0.022	0.082 \pm 0.015	0.097 \pm 0.014	0.132\pm0.005	0.113 \pm 0.013
2 000	0.165 \pm 0.019	0.130 \pm 0.026	0.183 \pm 0.032	0.232 \pm 0.017	0.291 \pm 0.012	0.304\pm0.035
3 000	0.197 \pm 0.012	0.142 \pm 0.025	0.257 \pm 0.049	0.399 \pm 0.058	0.376 \pm 0.022	0.403\pm0.050
5 000	0.410 \pm 0.041	0.261 \pm 0.044	0.592 \pm 0.037	0.447 \pm 0.045	0.659 \pm 0.018	0.699\pm0.047
8 000	0.691 \pm 0.067	0.467 \pm 0.038	0.892 \pm 0.029	0.878 \pm 0.020	0.923 \pm 0.013	0.952\pm0.024
10 000	0.786 \pm 0.041	0.603 \pm 0.066	0.974 \pm 0.007	0.985 \pm 0.005	1.000\pm0.000	1.000\pm0.000
Avg.	0.395	0.283	0.497	0.506	0.564	0.579

 Table 2. *MNIST* ($\alpha = 0.05$): average test power \pm standard error for comparing N real images to N DCGAN samples.

N	ME	SCF	C2ST-S	C2ST-L	MMD-O	MMD-D
200	0.414 \pm 0.050	0.107 \pm 0.018	0.193 \pm 0.037	0.234 \pm 0.031	0.188 \pm 0.010	0.555\pm0.044
400	0.921 \pm 0.032	0.152 \pm 0.021	0.646 \pm 0.039	0.706 \pm 0.047	0.363 \pm 0.017	0.996\pm0.004
600	1.000\pm0.000	0.294 \pm 0.008	1.000\pm0.000	0.977 \pm 0.012	0.619 \pm 0.021	1.000\pm0.000
800	1.000\pm0.000	0.317 \pm 0.017	1.000\pm0.000	1.000\pm0.000	0.797 \pm 0.015	1.000\pm0.000
1 000	1.000\pm0.000	0.346 \pm 0.019	1.000\pm0.000	1.000\pm0.000	0.894 \pm 0.016	1.000\pm0.000
Avg.	0.867	0.243	0.768	0.783	0.572	0.910

average Type I error (\mathbb{P} to \mathbb{P}) in Table 8 (in Appendix B.6). MMD-D substantially outperforms its competitors in test power, with the desired Type I error. ME also does well in this case: it is perhaps particularly suited to this problem, since it is capable of identifying either modes dropped by the generative model or spurious modes it inserts.

CIFAR-10 vs CIFAR-10.1. *CIFAR-10.1* (Recht et al., 2019) is an attempt to collect a new test set for the very popular *CIFAR-10* image classification dataset (Krizhevsky, 2009). Normally, when evaluating a supervised model, we consider the test set an independent sample from the training distribution, ideally never-before-seen by the training algorithm. But modern computer vision model architectures and training procedures have been developed based on repeatedly evaluating on the *CIFAR-10* test set (\mathbb{P}), so it is possible that current models themselves are dependent on \mathbb{P} . *CIFAR-10.1* (\mathbb{Q}) is an attempt at an independent sample from this distribution, collected after the models were trained, so that they are truly independent of \mathbb{Q} . These models do obtain substantially lower accuracies on \mathbb{Q} than on \mathbb{P} – but this drop is surprisingly consistent across models, which seems unlikely to be due to the expected overfitting. The main potential explanation proposed by Recht et al. is dataset shift, but their attempt (in their Appendix C.2.8) at what amounts to a C2ST-S did not reject \mathfrak{H}_0 .⁴ Samples from each distribution are shown in Figure 5 (Appendix B.2).

We train on 1 000 images from each dataset and test on 1 031, so that we use the entirety of *CIFAR-10.1* each time, and average over ten repetitions. These tests provide strong

⁴Assuming pretrained classifiers are independent of \mathbb{P} , Figure 1 of Recht et al. (2019) indicates that the joint (images, labels) distribution certainly differs between *CIFAR-10* and *CIFAR-10.1*. We test here whether the marginal image distribution differs.

 Table 3. *CIFAR-10.1* ($\alpha = 0.05$): mean rejection rates.

ME	SCF	C2ST-S	C2ST-L	MMD-O	MMD-D
0.588	0.171	0.452	0.529	0.316	0.744

evidence (Table 3) that images in the *CIFAR-10.1* test set are statistically different from the *CIFAR-10* test set, with MMD-D again strongest and ME still performing well.

Our learned kernel also helps provide some ability to interpret the difference between \mathbb{P} and \mathbb{Q} , particularly if we use it for an ME test. Appendix C explores this.

Recht et al. (2019) also provide a new ImageNetV2 test set for the ImageNet dataset, with similar properties; we defer this more challenging problem to future work.

7.2. Ablation Study

We now study in more detail the difference between MMD-D and closely related methods. Recall from Section 4 that there are two main differences between MMD-D and C2STs: first, using a “full” kernel (1) rather than the sign-based kernel (6) or the intermediate linear kernel (7). Second, training to maximize \hat{J}_λ (4) rather than a cross-entry surrogate. MMD-D uses a full kernel (1) trained for test power; C2ST-S effectively uses the sign kernel (6) trained for cross entropy.

In this section, we consider the performance of several intermediate models empirically, demonstrating that both factors help in testing. All are based on the same feature extraction architecture ϕ_ω ; some models add a classification layer with new parameters w and b ,

$$f_\omega(x) = w^\top \phi_\omega(x) + b,$$

Table 4. Mean test power on *Blob* ($n_b = 40$), *HDGM* ($N = 4000, d = 10$), *Higgs* ($N = 3000$) and *MNIST* ($N = 400$) for $\alpha = 0.05$. See Section 7.2 for the naming scheme; S+C corresponds to C2ST-S, L+C to C2ST-L, and D+J to MMD-D. L+M is the method proposed by Kirchler et al. (2020).

	S+C	L+C	G+C	D+C	L+M	G+M	D+M	L+J	G+J	D+J
<i>Blob</i>	0.835	0.942	0.901	0.900	0.851	0.960	0.906	0.952	0.966	0.985
<i>HDGM</i>	0.472	0.585	0.287	0.302	0.494	0.223	0.539	0.635	0.604	0.659
<i>Higgs</i>	0.257	0.399	0.353	0.384	0.321	0.254	0.379	0.295	0.364	0.403
<i>MNIST</i>	0.646	0.706	0.784	0.803	0.845	0.680	0.760	0.935	0.976	0.996
Avg.	0.553	0.658	0.581	0.597	0.628	0.529	0.646	0.704	0.727	0.761

Table 5. Paired t-test results ($\alpha = 0.05$) for the results of Section 7.1. For *HDGM*, we fix $d = 10$ (corresponding to Figure 3a). ✓ indicates MMD-D achieved statistically significantly higher mean test power than the other method, × that it did not.

Dataset	ME	SCF	C2ST-S	C2ST-L	MMD-O
<i>Blob</i>	✓	✓	✓	×	×
<i>HDGM</i>	✓	✓	✓	✓	✓
<i>Higgs</i>	✓	✓	✓	×	×
<i>MNIST</i>	✓	✓	✓	✓	✓

which is treated as outputting classification logits. The model variants we consider are

- S** A kernel $\mathbb{1}(f_\omega(x) > 0)\mathbb{1}(f_\omega(y) > 0)$; corresponds to a test statistic of the accuracy of f (Proposition 3).
- L** A kernel $f_\omega(x)f_\omega(y)$; corresponds to a test statistic comparing the mean value of f (Proposition 4).
- G** A Gaussian kernel $\kappa(\phi_\omega(x), \phi_\omega(y))$.
- D** The deep kernel (1) based on ϕ_ω .

We combine these model variants with a suffix describing the optimization objective:

- J** Choose ω , including possibly w and b , to optimize the approximate test power (4).
- M** Choose ω , including possibly w and b , to maximize the value of the empirical MMD between two samples.⁵
- C** Choose ω , including w and b , to optimize cross-entropy using the classifier that specifies the probability of x belonging to \mathbb{P} as $1/(1 + \exp(-f_\omega(x)))$.⁶

Table 4 presents results for all of these methods (except for S+J, which is non-differentiable and hence difficult to optimize). Performance generally improves as we move from S to L to G to D, and from C to J.

⁵If a deep kernel is unbounded, directly maximizing MMD will make optimized parameters of ϕ_ω be infinite. Thus, for L+M, we consider a normalized linear deep kernel: $\tanh(f_\omega(x)/\|S\|_F)\tanh(f_\omega(y)/\|S\|_F)$, where $S = [S_P; S_Q]$ and $\|\cdot\|_F$ is the Frobenius norm.

⁶G+C and D+C take the fixed ϕ_ω embeddings, then find the optimal lengthscale/etc by optimizing \hat{J}_λ .

7.3. Architecture design of deep kernels

For *Blob*, *HDGM* and *Higgs*, ϕ_ω is a five-layer fully-connected neural network, with softplus activations. the number of neurons in hidden and output layers of ϕ_ω are set to 50 for *Blob*, 3d for *HDGM* and 20 for *Higgs*, where d is the dimension of samples. in general, we expect similar fully-connected networks, to be reasonable choices for datasets where strong structural assumptions are not known, perhaps with 3d as a baseline width for datasets of at least moderate dimension.

For *MNIST* and *CIFAR*, ϕ_ω is a *convolutional neural network* (CNN) that contains four convolutional layers and one fully-connected layer. The structure of the CNN follows the structure of the feature extractor in the DCGAN’s discriminator (Radford et al., 2016) (see Figures 6 and 8 for the structure of ϕ_ω in MMD-D, and Figures 7 and 9 for the structure of classifier F in C2ST-S and C2ST-L). In general, we expect GAN discriminator architectures to work well for image datasets, as the problem is closely related.

8. Conclusions

The test power of MMD is limited by simple kernels (e.g., Gaussian kernel or other translation-invariant kernels) when facing complex-structured distributions, but we can avoid this problem with richer *deep kernels*, which is no longer translation-invariant. We show that optimizing the parameters of these kernels to maximize the test power, as proposed by Sutherland et al. (2017), outperforms state-of-the-art alternatives even when considering large, deep kernels with hundreds of thousands of parameters, rather than the simple shallow kernels they considered. We provide theoretical guarantees that this process is reasonable to conduct on finite samples, and asymptotically selects the most powerful kernel. We also give deeper insight into the relationship between this approach and classifier two-sample tests (Lopez-Paz & Oquab, 2017), explaining why this approach outperforms that one.

We thus recommend practitioners to use optimized deep kernel methods when they wish to check if two distributions are the same, rather than indirectly training a classifier.

Acknowledgements

This work was supported by the Australian Research Council under FL190100149 and DP170101632, and by the Gatsby Charitable Foundation. FL, JL and GZ gratefully acknowledge the support of the NVIDIA Corporation with the donation of two NVIDIA TITAN V GPUs for this work. FL also acknowledges the support from UTS-FEIT and UTS-AAII. DJS would like to thank Aram Ebtekar, Ameya Velingker, and Siddhartha Jain for productive discussions.

References

- Alba Fernández, V., Jiménez Gamero, M., and Muñoz García, J. A test for the two-sample problem based on empirical characteristic functions. *Computational Statistics & Data Analysis*, 52(7):3730–3748, 2008.
- Arbel, M., Sutherland, D. J., Binkowski, M., and Gretton, A. On gradient regularizers for MMD GANs. In *NeurIPS*, 2018.
- Baldi, P., Sadowski, P., and Whiteson, D. Searching for exotic particles in high-energy physics with deep learning. *Nature communications*, 5:4308, 2014.
- Berlinet, A. and Thomas-Agnan, C. *Reproducing Kernel Hilbert Spaces in Probability and Statistics*. Kluwer, 2004.
- Bibi, A., Ghanem, B., Koltun, V., and Ranftl, R. Deep layers as stochastic solvers. In *ICLR*, 2019.
- Binkowski, M., Sutherland, D. J., Arbel, M., and Gretton, A. Demystifying MMD GANs. In *ICLR*, 2018.
- Callaert, H. and Janssen, P. The Berry-Esseen theorem for u -statistics. *The Annals of Statistics*, 6(2):417–421, 1978.
- Chen, H. and Friedman, J. H. A new graph-based two-sample test for multivariate and object data. *Journal of the American Statistical Association*, 112(517):397–409, 2017.
- Chen, X. and Cloninger, A. Classification logit two-sample testing by neural networks, 2019. [arXiv:1909.11298](https://arxiv.org/abs/1909.11298).
- Chwialkowski, K., Ramdas, A., Sejdinovic, D., and Gretton, A. Fast two-sample testing with analytic representations of probability measures. In *NeurIPS*, 2015.
- Cucker, F. and Smale, S. On the mathematical foundations of learning. *Bulletin of the American Mathematical Society*, 39(1):1–49, 2001.
- Dwass, M. Modified randomization tests for nonparametric hypotheses. *The Annals of Mathematical Statistics*, 28(1):181–187, 03 1957.
- Gao, R., Xie, L., Xie, Y., and Xu, H. Robust hypothesis testing using Wasserstein uncertainty sets. In *NeurIPS*, 2018.
- Ghoshdastidar, D. and von Luxburg, U. Practical methods for graph two-sample testing. In *NeurIPS*, 2018.
- Ghoshdastidar, D., Gutzeit, M., Carpentier, A., and von Luxburg, U. Two-sample tests for large random graphs using network statistics. In *COLT*, 2017.
- Gönen, M. and Alpaydn, E. Multiple kernel learning algorithms. *Journal of Machine Learning Research*, 12: 2211–2268, 2011.
- Gong, M., Zhang, K., Liu, T., Tao, D., Glymour, C., and Systems, I. Domain adaptation with conditional transferable components. In *ICML*, 2016.
- Gretton, A., Fukumizu, K., Harchaoui, Z., and Sriperumbudur, B. K. A fast, consistent kernel two-sample test. In *NeurIPS*, 2009.
- Gretton, A., Borgwardt, K. M., Rasch, M. J., Schölkopf, B., and Smola, A. J. A kernel two-sample test. *Journal of Machine Learning Research*, 13:723–773, 2012a.
- Gretton, A., Sriperumbudur, B., Sejdinovic, D., Strathmann, H., and Pontil, M. Optimal kernel choice for large-scale two-sample tests. In *NeurIPS*, 2012b.
- Harchaoui, Z., Bach, F., and Moulines, E. Testing for homogeneity with kernel Fisher discriminant analysis. In *NeurIPS*, 2007.
- Heller, R. and Heller, Y. Multivariate tests of association based on univariate tests. In *NeurIPS*, 2016.
- Jean, N., Xie, S. M., and Ermon, S. Semi-supervised deep kernel learning: Regression with unlabeled data by minimizing predictive variance. In *NeurIPS*, 2018.
- Jitkrittum, W., Szabo, Z., Chwialkowski, K., and Gretton, A. Interpretable distribution features with maximum testing power. In *NeurIPS*, 2016.
- Jitkrittum, W., Xu, W., Szabo, Z., Fukumizu, K., and Gretton, A. A linear-time kernel goodness-of-fit test. In *NeurIPS*, 2017.
- Kim, I., Ramdas, A., Singh, A., and Wasserman, L. Classification accuracy as a proxy for two sample testing. *Annals of Statistics*, 2020. [arXiv:1602.02210](https://arxiv.org/abs/1602.02210).
- Kingma, D. P. and Ba, J. Adam: A method for stochastic optimization. In *ICLR*, 2015.
- Kirchler, M., Khorasani, S., Kloft, M., and Lippert, C. Two-sample testing using deep learning. In *AISTATS*, 2020. [arXiv:1910.06239](https://arxiv.org/abs/1910.06239).

- Korolyuk, V. S. and Borovskikh, Y. V. Asymptotic theory of U-statistics. *Ukrainian Mathematical Journal*, 40(2): 142–154, mar 1988.
- Krizhevsky, A. Learning multiple layers of features from tiny images, 2009. URL <https://www.cs.toronto.edu/~kriz/learning-features-2009-TR.pdf>.
- LeCun, Y., Bottou, L., Bengio, Y., Haffner, P., et al. Gradient-based learning applied to document recognition. *Proceedings of the IEEE*, 86(11):2278–2324, 1998.
- Li, C.-L., Chang, W.-C., Cheng, Y., Yang, Y., and Póczos, B. MMD GAN: Towards deeper understanding of moment matching network. In *NeurIPS*, 2017.
- Li, S. and Wang, X. Fully distributed sequential hypothesis testing: Algorithms and asymptotic analyses. *IEEE Trans. Information Theory*, 64(4):2742–2758, 2018.
- Lopez-Paz, D. and Oquab, M. Revisiting classifier two-sample tests. In *ICLR*, 2017.
- Muandet, K., Fukumizu, K., Sriperumbudur, B., and Schölkopf, B. Kernel mean embedding of distributions: A review and beyond. *Foundations and Trends® in Machine Learning*, 10(1-2):1–141, May 2017.
- Müller, A. Integral probability metrics and their generating classes of functions. *Advances in Applied Probability*, 29 (2):429–443, 1997.
- Radford, A., Metz, L., and Chintala, S. Unsupervised representation learning with deep convolutional generative adversarial networks. In *ICLR*, 2016.
- Ramdas, A., García Trillos, N., and Cuturi, M. On Wasserstein two-sample testing and related families of nonparametric tests. *Entropy*, 19(2):47, January 2017.
- Recht, B., Roelofs, R., Schmidt, L., and Shankar, V. Do ImageNet classifiers generalize to ImageNet? In *ICML*, 2019.
- Sedghi, H., Gupta, V., and Long, P. M. The singular values of convolutional layers. In *ICLR*, 2019.
- Serfling, R. J. *Approximation Theorems of Mathematical Statistics*. John Wiley & Sons, 1980.
- Smola, A. J. and Schölkopf, B. *Learning with Kernels: Support Vector Machines, Regularization, Optimization, and Beyond*. MIT Press, 2001.
- Sriperumbudur, B. K., Fukumizu, K., Gretton, A., Lanckriet, G. R., and Schölkopf, B. Kernel choice and classifiability for rkhs embeddings of probability distributions. In *NeurIPS*, 2009.
- Stojanov, P., Gong, M., Carbonell, J. G., and Zhang, K. Data-driven approach to multiple-source domain adaptation. In *AISTATS*, 2019.
- Sutherland, D. J. Unbiased estimators for the variance of MMD estimators, 2019. [arXiv:1906.02104](https://arxiv.org/abs/1906.02104).
- Sutherland, D. J., Tung, H.-Y., Strathmann, H., De, S., Ramdas, A., Smola, A., and Gretton, A. Generative models and model criticism via optimized maximum mean discrepancy. In *ICLR*, 2017.
- Székely, G. J. and Rizzo, M. L. Energy statistics: A class of statistics based on distances. *Journal of Statistical Planning and Inference*, 143(8):1249–1272, 2013.
- Torralba, A., Fergus, R., and Freeman, W. T. 80 million tiny images: A large data set for nonparametric object and scene recognition. *IEEE Transactions on Pattern Analysis and Machine Intelligence*, 30(11):1958–1970, 2008.
- Van der Vaart, A. W. *Asymptotic Statistics*. Cambridge University Press, 2000.
- Wenliang, L., Sutherland, D. J., Strathmann, H., and Gretton, A. Learning deep kernels for exponential family densities. In *ICML*, 2019.
- Wilson, A. G., Hu, Z., Salakhutdinov, R., and Xing, E. P. Deep kernel learning. In *AISTATS*, 2016.
- Zaremba, W., Gretton, A., and Blaschko, M. B-tests: Low variance kernel two-sample tests. In *NeurIPS*, 2013.

A. Theoretical analysis

Appendix A.2 proves the main results under some assumptions about the kernel parameterization, using intermediate results about uniform convergence of our estimators in Appendix A.3. Appendix A.4 then shows that these assumptions hold for different settings of kernel learning.

A.1. Preliminaries

Given a kernel k_ω and sample sets $\{X_i\}_{i=1}^n \sim \mathbb{P}^n$, $\{Y_i\}_{i=1}^n \sim \mathbb{Q}^n$, define the $n \times n$ matrix

$$H_{ij}^{(\omega)} = k_\omega(X_i, X_j) + k_\omega(Y_i, Y_j) - k_\omega(X_i, Y_j) - k_\omega(X_j, Y_i);$$

we will often omit ω when it is clear from context. The U -statistic estimator of the squared MMD (2) is

$$\hat{\eta}_\omega = \frac{1}{n(n-1)} \sum_{i \neq j} H_{ij}.$$

The squared MMD is $\eta_\omega = \mathbb{E}[H_{12}]$. The variance of $\hat{\eta}_\omega$ is given by Lemma 10.

Lemma 10. *For a fixed kernel k_ω and random sample sets $\{X_i\}_{i=1}^n$, $\{Y_i\}_{i=1}^n$, we have*

$$\text{Var}[\hat{\eta}_\omega] = \frac{4(n-2)}{n(n-1)} \xi_1^{(\omega)} + \frac{2}{n(n-1)} \xi_2^{(\omega)} = \frac{4}{n} \xi_1^{(\omega)} + \frac{2\xi_2^{(\omega)} - 4\xi_1^{(\omega)}}{n(n-1)}, \quad (8)$$

where

$$\xi_1^{(\omega)} = \mathbb{E} \left[H_{12}^{(\omega)} H_{13}^{(\omega)} \right] - \mathbb{E} \left[H_{12}^{(\omega)} \right]^2, \quad \xi_2^{(\omega)} = \mathbb{E} \left[\left(H_{12}^{(\omega)} \right)^2 \right] - \mathbb{E} \left[H_{12}^{(\omega)} \right]^2.$$

Thus as $n \rightarrow \infty$,

$$n \text{Var}[\hat{\eta}_\omega] \rightarrow 4\xi_1^{(\omega)} =: \sigma_\omega^2.$$

Proof. Let U denote the pair (X, Y) , and $h_\omega(U, U') = k_\omega(X, X') + k_\omega(Y, Y') - k_\omega(X, Y') - k_\omega(X', Y)$, so that $H_{ij}^{(\omega)} = h_\omega(U_i, U_j)$. Via Lemma A in Section 5.2.1 of Serfling (1980), we know that (8) holds with

$$\begin{aligned} \xi_1^{(\omega)} &= \text{Var}_U [\mathbb{E}_{U'} [h_\omega(U, U')]] \\ &= \mathbb{E}_U [\mathbb{E}_{U'} [h_\omega(U, U')] \mathbb{E}_{U''} [h_\omega(U, U'')]] - \mathbb{E}_U [\mathbb{E}_{U'} [h_\omega(U, U')]]^2 \\ &= \mathbb{E}[H_{12}^{(\omega)} H_{13}^{(\omega)}] - \mathbb{E}[H_{12}^{(\omega)}]^2 \end{aligned}$$

and

$$\xi_2 = \text{Var}_{U, U'} [h_\omega(U, U')] = \mathbb{E} \left[\left(H_{12}^{(\omega)} \right)^2 \right] - \mathbb{E} \left[H_{12}^{(\omega)} \right]^2. \quad \square$$

We use a V -statistic estimator (5) for σ_ω^2 :

$$\hat{\sigma}_\omega^2 = 4 \left(\frac{1}{n} \sum_{i=1}^n \left(\frac{1}{n} \sum_{j=1}^n H_{ij}^{(\omega)} \right)^2 - \left(\frac{1}{n^2} \sum_{i=1}^n \sum_{j=1}^n H_{ij}^{(\omega)} \right)^2 \right).$$

As a V -statistic, $\hat{\sigma}_\omega^2$ is biased. In fact, Sutherland et al. (2017) and Sutherland (2019) provide an unbiased estimator of $\text{Var}[\hat{\eta}_\omega]$ – including the terms of order $\frac{1}{n(n-1)}$. Although this estimator takes the same quadratic time to compute as (5), it contains many more terms, which are cumbersome both for implementation and for analysis. (5) is also marginally more convenient in that it is always at least nonnegative. As we show in Lemma 18, the amount of bias is negligible as n increases. In practice, we expect the difference to be unimportant – or the V -statistic may in fact be beneficial, since underestimating σ^2 harms the estimate of η/σ^2 more than overestimating it does.

Similarly, although we use the U -statistic estimator (2), it would be very similar to use the biased estimator $n^{-2} \sum_{i,j} H_{ij}$, or the minimum variance unbiased estimator $n^{-1}(n-1)^{-1} \sum_{i \neq j} (k(X_i, X_j) + k(Y_i, Y_j)) - 2n^{-2} \sum_{i,j} k(X_i, Y_j)$. Showing comparable concentration behavior to Proposition 15 is trivially different, and in fact it is also not difficult to show σ_ω^2 is the same for all three estimators (up to lower-order terms).

A.2. Main results

We will require the following assumptions. These are fairly agnostic as to the kernel form; Appendix A.4.2 shows that these assumptions hold (and gives the constants) for the kernels (1) we use in the paper.

(A) The kernels k_ω are uniformly bounded:

$$\sup_{\omega \in \Omega} \sup_{x \in \mathcal{X}} k_\omega(x, x) \leq \nu.$$

For the kernels we use in practice, $\nu = 1$.

(B) The possible kernel parameters ω lie in a Banach space of dimension D . Furthermore, the set of possible kernel parameters Ω is bounded by R_ω , $\Omega \subseteq \{\omega \mid \|\omega\| \leq R_\Omega\}$.

Appendix A.4.2 builds this space and its norm for the kernels we use in the paper.

(C) The kernel parameterization is Lipschitz: for all $x, y \in \mathcal{X}$ and $\omega, \omega' \in \Omega$,

$$|k_\omega(x, y) - k_{\omega'}(x, y)| \leq L_k \|\omega - \omega'\|.$$

Proposition 23 in Appendix A.4.2 gives an expression for L_k for the kernels we use in the paper.

We will first show the main results under these general assumptions, using uniform convergence results shown in Appendix A.3, then show Assumptions (B) and (C) for particular kernels in Appendix A.4.2.

Theorem 11. *Under Assumptions (A) to (C), let $\bar{\Omega}_s \subseteq \Omega$ be the set of kernel parameters for which $\sigma_\omega^2 \geq s^2$, and assume $\nu \geq 1$. Take $\lambda = n^{-1/3}$. Then, with probability at least $1 - \delta$,*

$$\sup_{\omega \in \bar{\Omega}_s} \left| \frac{\hat{\eta}_\omega}{\hat{\sigma}_{\omega, \lambda}} - \frac{\eta_\omega}{\sigma_\omega} \right| \leq \frac{2\nu}{s^2 n^{1/3}} \left(\frac{1}{s} + \frac{2304\nu^2}{\sqrt{n}} + \left[\frac{4s}{n^{1/6}} + 1024\nu \right] \left[L_k + \sqrt{2 \log \frac{2}{\delta} + 2D \log(4R_\Omega \sqrt{n})} \right] \right),$$

and thus, treating ν as a constant,

$$\sup_{\omega \in \bar{\Omega}_s} \left| \frac{\hat{\eta}_\omega}{\hat{\sigma}_{\omega, \lambda}} - \frac{\eta_\omega}{\sigma_\omega} \right| = \tilde{O}_P \left(\frac{1}{s^2 n^{1/3}} \left[\frac{1}{s} + L_k + \sqrt{D} \right] \right).$$

Proof. Let $\sigma_{\omega, \lambda}^2 := \sigma_\omega^2 + \lambda$. Using $|\hat{\eta}_\omega| \leq 4\nu$, we begin by decomposing

$$\begin{aligned} \sup_{\omega \in \bar{\Omega}_s} \left| \frac{\hat{\eta}_\omega}{\hat{\sigma}_{\omega, \lambda}} - \frac{\eta_\omega}{\sigma_\omega} \right| &\leq \sup_{\omega \in \bar{\Omega}_s} \left| \frac{\hat{\eta}_\omega}{\hat{\sigma}_{\omega, \lambda}} - \frac{\hat{\eta}_\omega}{\sigma_{\omega, \lambda}} \right| + \sup_{\omega \in \bar{\Omega}_s} \left| \frac{\hat{\eta}_\omega}{\sigma_{\omega, \lambda}} - \frac{\hat{\eta}_\omega}{\sigma_\omega} \right| + \sup_{\omega \in \bar{\Omega}_s} \left| \frac{\hat{\eta}_\omega}{\sigma_\omega} - \frac{\eta_\omega}{\sigma_\omega} \right| \\ &= \sup_{\omega \in \bar{\Omega}_s} |\hat{\eta}_\omega| \frac{1}{\hat{\sigma}_{\omega, \lambda}} \frac{1}{\sigma_{\omega, \lambda}} \frac{|\hat{\sigma}_{\omega, \lambda}^2 - \sigma_{\omega, \lambda}^2|}{\hat{\sigma}_{\omega, \lambda} + \sigma_{\omega, \lambda}} + \sup_{\omega \in \bar{\Omega}_s} |\hat{\eta}_\omega| \frac{1}{\sigma_{\omega, \lambda}} \frac{1}{\sigma_\omega} \frac{|\sigma_{\omega, \lambda}^2 - \sigma_\omega^2|}{\sigma_{\omega, \lambda} + \sigma_\omega} + \sup_{\omega \in \bar{\Omega}_s} \frac{1}{\sigma_\omega} |\hat{\eta}_\omega - \eta_\omega| \\ &\leq \sup_{\omega \in \bar{\Omega}_s} \frac{4\nu}{\sqrt{\lambda} s (s + \sqrt{\lambda})} |\hat{\sigma}_\omega^2 - \sigma_\omega^2| + \frac{4\nu \lambda}{\sqrt{s^2 + \lambda} s (\sqrt{s^2 + \lambda} + s)} + \sup_{\omega \in \bar{\Omega}_s} \frac{1}{s} |\hat{\eta}_\omega - \eta_\omega| \\ &\leq \frac{4\nu}{s^2 \sqrt{\lambda}} \sup_{\omega \in \bar{\Omega}} |\hat{\sigma}_\omega^2 - \sigma_\omega^2| + \frac{2\nu}{s^3} \lambda + \frac{1}{s} \sup_{\omega \in \bar{\Omega}} |\hat{\eta}_\omega - \eta_\omega|. \end{aligned}$$

Propositions 15 and 16 show uniform convergence of $\hat{\eta}_\omega$ and $\hat{\sigma}_\omega^2$, respectively. Thus, with probability at least $1 - \delta$, the error is at most

$$\frac{2\nu}{s^3} \lambda + \left[\frac{8\nu}{s\sqrt{n}} + \frac{1792\nu}{\sqrt{n}s^2\sqrt{\lambda}} \right] \sqrt{2 \log \frac{2}{\delta} + 2D \log(4R_\Omega \sqrt{n})} + \left[\frac{8}{s\sqrt{n}} + \frac{2048\nu^2}{\sqrt{n}s^2\sqrt{\lambda}} \right] L_k + \frac{4608\nu^3}{s^2 n \sqrt{\lambda}}.$$

Taking $\lambda = n^{-1/3}$ gives

$$\frac{2\nu}{s^3 n^{1/3}} + \left[\frac{8\nu}{s\sqrt{n}} + \frac{1792\nu}{s^2 n^{1/3}} \right] \sqrt{2 \log \frac{2}{\delta} + 2D \log(4R_\Omega \sqrt{n})} + \left[\frac{8}{s\sqrt{n}} + \frac{2048\nu^2}{s^2 n^{1/3}} \right] L_k + \frac{4608\nu^3}{s^2 n^{5/6}}.$$

Using $1 \leq \nu$, $1792 < 2048$, we can get the slightly simpler upper bound

$$\frac{2\nu}{s^3 n^{1/3}} + \left[\frac{8\nu}{s\sqrt{n}} + \frac{2048\nu^2}{s^2 n^{1/3}} \right] \left[L_k + \sqrt{2 \log \frac{2}{\delta} + 2D \log(4R_\Omega \sqrt{n})} \right] + \frac{4608\nu^3}{s^2 n^{5/6}}. \quad \square$$

It is worth noting that, if we are particularly concerned about the s dependence, we can make some slightly different choices in the decomposition to improve the dependence on s while worsening the rate with n .

Corollary 12. *In the setup of Theorem 11, additionally assume that there is a unique population maximizer ω^* of J from (3), i.e. for each $t > 0$ we have*

$$\sup_{\omega \in \bar{\Omega}_s : \|\omega - \omega^*\| \geq t} J(\mathbb{P}, \mathbb{Q}; k_\omega) < J(\mathbb{P}, \mathbb{Q}; k_{\omega^*}).$$

For each n , let $S_{\mathbb{P}}^{(n)}$ and $S_{\mathbb{Q}}^{(n)}$ be sequences of sample sets of size n , let $\hat{J}_n(\omega)$ denote $J_{\lambda=n^{-1/3}}(S_{\mathbb{P}}^{(n)}, S_{\mathbb{Q}}^{(n)}; k_\omega)$, and take $\hat{\omega}_n^*$ to be a maximizer of $\hat{J}_n(\omega)$.⁷ Then $\hat{\omega}_n^*$ converges in probability to ω^* .

Proof. By Theorem 11, $\sup_{\omega \in \bar{\Omega}_s} |\hat{J}_n(\omega) - J(\omega)| \xrightarrow{P} 0$. Then the result follows by Theorem 5.7 of Van der Vaart (2000). \square

Corollary 13. *In the setup of Theorem 11, suppose we use n sample points to select a kernel $\hat{\omega}_n \in \arg \max_{\omega \in \bar{\Omega}_s} \hat{J}_\lambda(\omega)$ and m sample points to run a test of level α . Let $r_{\hat{\omega}_n}^{(m)}$ denote the rejection threshold for a test with that kernel of size m . Define $J^* := \sup_{\omega \in \bar{\Omega}_s} J(\omega)$, and constants C, C', C'', N_0 depending on ν, L_k, D, R_Ω and s . For any $n \geq N_0$, with probability at least $1 - \delta$, this test procedure has power*

$$\Pr \left(m \hat{\omega}_n > r_{\hat{\omega}_n}^{(m)} \right) \geq \Phi \left(\sqrt{m} J^* - C \frac{\sqrt{m}}{n^{1/3}} \sqrt{\log \frac{n}{\delta}} - C' \sqrt{\log \frac{1}{\alpha}} \right) - \frac{C''}{\sqrt{m}}.$$

Proof. Let $\hat{\omega}_n \in \arg \max_{\omega \in \bar{\Omega}_s} \hat{J}_\lambda(\omega)$. By Theorem 11, there are some N_0, C depending on ν, L_k, D, R_Ω , and s such that as long as $n \geq N_0$, with probability at least $1 - \delta$ it holds that

$$\sup_{\omega \in \bar{\Omega}_s} |J_\lambda(\omega) - J(\omega)| \leq \frac{1}{2} C n^{-1/3} \sqrt{\log \frac{n}{\delta}} =: \epsilon_n.$$

Assume for the remainder of this proof that this event holds. Letting $\omega^* \in \arg \max J(\omega)$, we know because $\hat{\omega}_n$ maximizes \hat{J}_λ that $\hat{J}_\lambda(\hat{\omega}_n) \geq \hat{J}_\lambda(\omega^*)$. Using uniform convergence twice,

$$J(\hat{\omega}_n) \geq \hat{J}_\lambda(\hat{\omega}_n) - \epsilon_n \geq \hat{J}_\lambda(\omega^*) - \epsilon_n \geq (J(\omega^*) - \epsilon_n) - \epsilon_n = J^* - 2\epsilon_n.$$

Now, although Proposition 2 establishes that $r_\omega^{(m)} \rightarrow r_\omega$ and it is even known (Korolyuk & Borovskikh, 1988, Theorem 5) that $|r_\omega^{(m)} - r_\omega|$ is $o(1/\sqrt{m})$, the constant in that convergence will depend on the choice of ω in an unknown way. It's thus simpler to use the very loose but uniform (McDiarmid-based) bound given by Corollary 11 of Gretton et al. (2012a), which implies $r_\omega^{(m)} \leq 4\nu \sqrt{\log(\alpha^{-1})m}$ no matter the choice of ω .

We will now need a more precise characterization of the power than that provided by the central limit theorem of Proposition 2. Callaert & Janssen (1978) provide such a result, a Berry-Esseen bound on U -statistic convergence: there is some absolute constant $C'_{BS} = 2^3 4^3 C_{BS}$ such that

$$\sup_t \left| \Pr \left(\sqrt{m} \frac{\hat{\eta}_\omega - \eta_\omega}{\sigma_\omega^2} \leq t \right) - \Phi(t) \right| \leq \frac{C'_{BS} \mathbb{E}|H_{12}|^3}{(\sigma_\omega/2)^3 \sqrt{m}} \leq \frac{C_{BS} \nu^3}{\sigma_\omega^3 \sqrt{m}}.$$

⁷In fact, it suffices for the $\hat{\omega}_n^*$ to only approximately maximize \hat{J}_n , as long as their suboptimality is $o_P(1)$.

Letting $r_\omega^{(m)}$ be the appropriate rejection threshold for k_ω with m samples, the power of a test with kernel k_ω is

$$\begin{aligned} \Pr \left(m\hat{\eta}_\omega > r_\omega^{(m)} \right) &= \Pr \left(\sqrt{m} \frac{\hat{\eta}_\omega - \eta_\omega}{\sigma_\omega} > \frac{r_\omega^{(m)}}{\sqrt{m}\sigma_\omega} - \sqrt{m} \frac{\eta_\omega}{\sigma_\omega} \right) \\ &\geq \Phi \left(\sqrt{m} J(\omega) - \frac{r_\omega^{(m)}}{\sqrt{m}\sigma_\omega} \right) - \frac{C_{BS}\nu^3}{\sigma_\omega^3 \sqrt{m}} \\ &\geq \Phi \left(\sqrt{m} J(\omega) - \frac{r_\omega^{(m)}}{s\sqrt{m}} \right) - \frac{C''}{\sqrt{m}}, \end{aligned}$$

using a new constant $C'' := C_{BS}\nu^3/s^3$. Combining the previous results on $J(\hat{\omega}_n)$ and $r_{\hat{\omega}_n}^{(m)}$ yields the claim. \square

Corollary 14. *In the setup of Corollary 13, suppose we are given N data points to divide between n training points and $m = N - n$ testing points, and $\delta < 0.22$ is fixed. Ignoring the Berry-Esseen convergence term outside of Φ , the asymptotic power upper bound*

$$\Phi \left(\sqrt{m} J^* - C \frac{\sqrt{m}}{n^{\frac{1}{3}}} \sqrt{\log \frac{n}{\delta}} - C' \sqrt{\log \frac{1}{\alpha}} \right)$$

is maximized only when, as other quantities remain constant, we pick n to satisfy

$$\lim_{N \rightarrow \infty} \frac{n}{\left(\frac{C}{\sqrt{3}J^*} N \sqrt{\log N} \right)^{\frac{3}{4}}} = 1.$$

Proof. Because the C' term is constant, we wish to choose

$$\arg \max_{0 < n < N} \frac{J^*}{C} \sqrt{N-n} - \frac{\sqrt{N-n}}{n^{\frac{1}{3}}} \sqrt{\log \frac{n}{\delta}}.$$

Clearly neither endpoint is optimal. Relaxing n to be real-valued, the optimum must be achieved at a stationary point, where

$$\frac{-J^*}{2C\sqrt{N-n}} + \frac{\sqrt{\log \frac{n}{\delta}}}{2\sqrt{N-n}n^{\frac{1}{3}}} + \frac{1}{3}\sqrt{N-n}n^{-\frac{4}{3}}\sqrt{\log \frac{n}{\delta}} - \frac{1}{2}\sqrt{N-n}n^{-\frac{4}{3}}\left(\log \frac{n}{\delta}\right)^{-\frac{1}{2}} = 0.$$

Multiplying by $2\sqrt{N-n}n^{\frac{4}{3}}\sqrt{\log \frac{n}{\delta}}$ and rearranging, we get that a stationary point is achieved exactly when

$$\underbrace{\frac{1}{3}[n+2N]\log \frac{n}{\delta} + n}_D = \underbrace{\frac{J^*}{C}n^{\frac{4}{3}}\sqrt{\log \frac{n}{\delta}} + N}_E.$$

Now write, without loss of generality, $n = (A_N N \sqrt{\log N})^{\frac{3}{4}}$, and so

$$\begin{aligned} D &= \frac{1}{3} \left[A_N^{\frac{3}{4}} N^{\frac{3}{4}} (\log N)^{\frac{3}{8}} + 2N \right] \left[\underbrace{\frac{3}{4} \log A_N + \frac{3}{4} \log N + \frac{3}{8} \log \log N + \log \frac{1}{\delta}}_{\log n} \right] + A_N^{\frac{3}{4}} N^{\frac{3}{4}} (\log N)^{\frac{3}{8}} \\ E &= \frac{J^*}{C} A_N N \sqrt{\log N} \sqrt{\underbrace{\frac{3}{4} \log A_N + \frac{3}{4} \log N + \frac{3}{8} \log \log N + \log \frac{1}{\delta}}_{\log n}} + N. \end{aligned}$$

We will show that $D - E \rightarrow 0$ requires $A_N \rightarrow C/(\sqrt{3}J^*)$, implying the result.

We first suppose $A_N = \omega(1)$, further breaking into cases which result in different terms inside D and E becoming dominant:

$$\text{If } A_N = \Omega(N), \quad D = \Theta \left(A_N^{\frac{3}{4}} N^{\frac{3}{4}} (\log N)^{\frac{3}{8}} \log A_N \right), \quad E = \Theta \left(A_N N \sqrt{\log(N) \log(A_N)} \right).$$

$$\text{If } A_N = \Omega \left(\frac{N^{\frac{1}{3}}}{\sqrt{\log N}} \right), A_N = o(N), \quad D = \Theta \left(A_N^{\frac{3}{4}} N^{\frac{3}{4}} (\log N)^{\frac{3}{8}} \log N \right), \quad E = \Theta(A_N N \log N).$$

$$\text{If } A_N = \omega(1), A_N = o \left(\frac{N^{\frac{1}{3}}}{\sqrt{\log N}} \right), \quad D = \Theta(N \log N), \quad E = \Theta(A_N N \log N).$$

In each case, $E = \omega(D)$ and so $D - E \rightarrow -\infty$, contradicting that $D = E$. Thus a stationary point requires $A_N = \mathcal{O}(1)$ for a stationary point.

We now do the same for $A_N = o(1)$. First, clearly $n \geq 1$; suppose that in fact $n = \Theta(1)$, i.e. $A_N = \Theta(1/(N\sqrt{\log N}))$. In this case, we would have $D = \frac{2}{3}N \log \frac{n}{\delta} + \Theta(1)$ and $E = N + \Theta(1)$, so that $D = E$ requires $\frac{2}{3} \log \frac{n}{\delta} \rightarrow 1$, i.e. $n \rightarrow \delta \exp \frac{3}{2} \approx 4.5 \delta$. For $\delta < 0.22$, this contradicts $n \geq 1$. So we know that $\log n = \omega(1)$. Now, the remaining options for A_N all yield $D - E \rightarrow \infty$:

$$\text{If } A_N = o(1), A_N = \Omega \left(\frac{1}{\log N} \right), \quad D = \Theta(N \log n), \quad E = \Theta(A_N N \log n).$$

$$\text{If } A_N = o \left(\frac{1}{\log N} \right), A_N = \omega \left(\frac{1}{N\sqrt{\log N}} \right), \quad D = \Theta(N \log n), \quad E = \Theta(N).$$

Thus we have established that $A_N = \Theta(1)$. Thus, we obtain that

$$D = \frac{1}{2}N \log N + \mathcal{O}(N) \quad E = \frac{\sqrt{3}J^*}{2C} A_N N \log N + \mathcal{O}(N \sqrt{\log N}).$$

Asymptotic equality hence requires $A_N \rightarrow C/(\sqrt{3}J^*)$. □

A.3. Uniform convergence results

These results, on the uniform convergence of $\hat{\eta}$ and $\hat{\sigma}^2$, were used in the proof of Theorem 11.

Proposition 15. *Under Assumptions (A) to (C), we have that with probability at least $1 - \delta$,*

$$\sup_{\omega} |\hat{\eta}_{\omega} - \eta_{\omega}| \leq \frac{8}{\sqrt{n}} \left[\nu \sqrt{2 \log \frac{2}{\delta} + 2D \log(4R_{\Omega} \sqrt{n})} + L_k \right].$$

Proof. Theorem 7 of [Sriperumbudur et al. \(2009\)](#) gives a similar bound in terms of Rademacher chaos complexity, but for ease of combination with our bound on convergence of the variance estimator, we use a simple ϵ -net argument instead.

We study the random error function

$$\Delta(\omega) := \hat{\eta}_{\omega} - \eta_{\omega}.$$

First, we place T points $\{\omega_i\}_{i=1}^T$ such that for any point $\omega \in \Omega$, $\min_i \|\omega - \omega_i\| \leq q$; Assumption (B) ensures this is possible with at most $T = (4R_{\Omega}/q)^D$ points ([Cucker & Smale, 2001](#), Proposition 5).

Now, $\mathbb{E} \Delta = 0$, because $\hat{\eta}$ is unbiased. Recall that $\hat{\eta} = \frac{1}{n(n-1)} \sum_{i \neq j} H_{ij}$, and via Assumption (A) we know $|H_{ij}| \leq 4\nu$. This $\hat{\eta}$, and hence Δ , satisfies bounded differences: if we replace (X_1, Y_1) with (X'_1, Y'_1) , obtaining $\hat{\eta}' = \frac{1}{n(n-1)} \sum_{i \neq j} F_{ij}$ where F agrees with H except when i or j is 1, then

$$\begin{aligned} |\hat{\eta} - \hat{\eta}'| &\leq \frac{1}{n(n-1)} \sum_{i \neq j} |H_{ij} - F_{ij}| = \frac{1}{n(n-1)} \sum_{i>1} |H_{i1} - F_{i1}| + \frac{1}{n(n-1)} \sum_{j>1} |H_{1j} - F_{1j}| \\ &\leq \frac{2}{n(n-1)} \sum_{i>1} 8\nu = \frac{16\nu}{n}. \end{aligned}$$

Using McDiarmid's inequality for each $\Delta(\omega_i)$ and a union bound, we then obtain that with probability at least $1 - \delta$,

$$\max_{i \in \{1, \dots, T\}} |\Delta(\omega_i)| \leq \frac{16\nu}{\sqrt{2n}} \sqrt{\log \frac{2T}{\delta}} \leq \frac{8\nu}{\sqrt{n}} \sqrt{2 \log \frac{2}{\delta} + 2D \log \frac{4R_\Omega}{q}}.$$

We also have via Assumption (C), for any two $\omega, \omega' \in \Omega$,

$$\begin{aligned} |\hat{\eta}_\omega - \hat{\eta}_{\omega'}| &\leq \frac{1}{n(n-1)} \sum_{i \neq j} |H_{ij}^{(\omega)} - H_{ij}^{(\omega')}| \leq \frac{1}{n(n-1)} \sum_{i \neq j} 4L_k \|\omega - \omega'\| = 4L_k \|\omega - \omega'\| \\ |\eta_\omega - \eta_{\omega'}| &= |\mathbb{E}[H_{12}^{(\omega)}] - \mathbb{E}[H_{12}^{(\omega')}]| \leq \mathbb{E}|H_{12}^{(\omega)} - H_{12}^{(\omega')}| \leq 4L_k \|\omega - \omega'\| \end{aligned}$$

so that $\|\Delta\|_L \leq 8L_k$. Combining these two results, we know that with probability at least $1 - \delta$

$$\sup_{\omega} |\Delta(\omega)| \leq \max_{i \in \{1, \dots, T\}} |\Delta(\omega_i)| + 8L_k q \leq \frac{8\nu}{\sqrt{n}} \sqrt{2 \log \frac{2}{\delta} + 2D \log \frac{4R_\Omega}{q}} + 8L_k q;$$

setting $q = 1/\sqrt{n}$ yields the desired result. \square

Proposition 16. *Under Assumptions (A) to (C), with probability at least $1 - \delta$,*

$$\sup_{\omega \in \Omega} |\hat{\sigma}_\omega^2 - \sigma_\omega^2| \leq \frac{64}{\sqrt{n}} \left[7 \sqrt{2 \log \frac{2}{\delta} + 2D \log (4R_\Omega \sqrt{n})} + \frac{18\nu^2}{\sqrt{n}} + 8L_k \nu \right].$$

Proof. We again use an ϵ -net argument on the (random) error function

$$\Delta(\omega) := \hat{\sigma}_{k_\omega}^2 - \sigma_{k_\omega}^2.$$

First, choose T points $\{\omega_i\}_{i=1}^T$ such that for any point $\omega \in \Omega$, $\min_i \|\omega - \omega_i\| \leq q$; again, via Assumption (B) and Proposition 5 of Cucker & Smale (2001) we have $T \leq (4R_\Omega/q)^D$. By Lemmas 17 and 18 and a union bound, with probability at least $1 - \delta$,

$$\max_{i \in \{1, \dots, T\}} |\Delta(\omega_i)| \leq 448 \sqrt{\frac{2}{n} \log \frac{2T}{\delta}} + \frac{1152\nu^2}{n} \leq 448 \sqrt{\frac{2}{n} \log \frac{2}{\delta} + \frac{2}{n} D \log \frac{4R_\Omega}{q}} + \frac{1152\nu^2}{n}.$$

Lemma 19 shows that $\|\Delta\|_L \leq 512L_k\nu$, which means that with probability at least $1 - \delta$,

$$\sup_{\omega \in \Omega} |\Delta(\omega)| \leq 448 \sqrt{\frac{2}{n} \log \frac{2}{\delta} + \frac{2}{n} D \log \frac{4R_\Omega}{q}} + \frac{1152\nu^2}{n} + 512L_k\nu q. \quad (9)$$

Taking $q = 1/\sqrt{n}$ gives the desired result. \square

Lemma 17. *For any kernel k bounded by ν (Assumption (A)), with probability at least $1 - \delta$,*

$$|\hat{\sigma}_k^2 - \mathbb{E} \hat{\sigma}_k^2| \leq 448 \sqrt{\frac{2}{n} \log \frac{2}{\delta}}.$$

Proof. We simply apply McDiarmid's inequality to $\hat{\sigma}_k^2$. Suppose we change (X_1, Y_1) to (X'_1, Y'_1) , giving a new H matrix F which agrees with H on all but the first row and column. Note that $|H_{ij}| \leq 4\nu$, and recall

$$\hat{\sigma}_k^2 = 4 \left(\frac{1}{n^3} \sum_i \left(\sum_j H_{ij} \right)^2 - \left(\frac{1}{n^2} \sum_{ij} H_{ij} \right)^2 \right).$$

The first term in the parentheses of $\hat{\sigma}_k^2$ changes by

$$\left| \frac{1}{n^3} \sum_i \left(\sum_j H_{ij} \right)^2 - \frac{1}{n^3} \sum_i \left(\sum_j F_{ij} \right)^2 \right| \leq \frac{1}{n^3} \sum_{ij\ell} |H_{ij}H_{i\ell} - F_{ij}F_{i\ell}|.$$

In this sum, if none of i, j , or ℓ are one, the term is zero. The n^2 terms for which $i = 1$ are each upper-bounded by $32\nu^2$, simply bounding each H or F by 4ν . Of the remainder, there are $(n-1)$ terms where $j = \ell = 1$, each $|H_{i1}^2 - F_{i1}^2| \leq 16\nu^2$. We are left with $2(n-1)^2$ terms which have exactly one of j or ℓ equal to 1; the $j = 1$ terms are $|H_{i1}H_{i\ell} - F_{i1}H_{i\ell}| \leq |H_{i1} - F_{i1}||H_{i\ell}| \leq (8\nu)(4\nu)$, so each of these terms is at most $32\nu^2$. The total sum is thus at most

$$\frac{1}{n^3} (n^2 32\nu^2 + (n-1)16\nu^2 + 2(n-1)^2 32\nu^2) = \left(\frac{6}{n} - \frac{7}{n^2} + \frac{3}{n^3} \right) 16\nu^2.$$

The remainder of the change in $\hat{\sigma}_k^2$ can be determined by bounding

$$\begin{aligned} \left| \sum_{ij} H_{ij} - \sum_{ij} F_{ij} \right| &\leq \sum_{ij} |H_{ij} - F_{ij}| = \sum_j |H_{1j} - F_{1j}| + \sum_{i>1} |H_{i1} - F_{i1}| \\ &\leq n(8\nu) + (n-1)(8\nu) = (8\nu)(2n-1), \end{aligned}$$

which then gives us

$$\begin{aligned} \left| \left(\frac{1}{n^2} \sum_{ij} H_{ij} \right)^2 - \left(\frac{1}{n^2} \sum_{ij} F_{ij} \right)^2 \right| &= \left| \frac{1}{n^2} \sum_{ij} H_{ij} + \frac{1}{n^2} \sum_{ij} F_{ij} \right| \left| \frac{1}{n^2} \sum_{ij} H_{ij} - \frac{1}{n^2} \sum_{ij} F_{ij} \right| \\ &\leq (2 \cdot 4\nu) \frac{2n-1}{n^2} (8\nu) = 64\nu^2 \left(\frac{2}{n} - \frac{1}{n^2} \right). \end{aligned}$$

Thus

$$|\hat{\sigma}_k^2 - (\hat{\sigma}'_k)^2| \leq 4 \left[\left(\frac{6}{n} - \frac{7}{n^2} + \frac{3}{n^3} \right) 16\nu^2 + \left(\frac{2}{n} - \frac{1}{n^2} \right) 64\nu^2 \right] = \frac{64\nu^2}{n^3} [14n^2 - 11n + 3] \leq \frac{896\nu^2}{n}.$$

Because the same holds for changing any of the (X_i, Y_i) pairs, the result follows by McDiarmid's inequality. \square

Lemma 18. *For any kernel k bounded by ν (Assumption (A)), the estimator $\hat{\sigma}_k^2$ satisfies*

$$|\mathbb{E} \hat{\sigma}_k^2 - \sigma_k^2| \leq \frac{1152\nu^2}{n}.$$

Proof. We have that

$$\mathbb{E} \hat{\sigma}_k^2 = 4 \left(\frac{1}{n^3} \sum_{ij\ell} \mathbb{E} [H_{i\ell} H_{j\ell}] - \frac{1}{n^4} \sum_{ijab} \mathbb{E} [H_{ij} H_{ab}] \right).$$

Most terms in these sums have their indices distinct; these are the ones that we care about. (We could evaluate the expectations of the other terms exactly, but it would be tedious.) We can thus break down the first term as

$$\begin{aligned} \frac{1}{n^3} \sum_{ij\ell} \mathbb{E} [H_{i\ell} H_{j\ell}] &= \frac{1}{n^3} \sum_{ij\ell: |\{i,j,\ell\}|=3} \mathbb{E} [H_{i\ell} H_{j\ell}] + \frac{1}{n^3} \sum_{ij\ell: |\{i,j,\ell\}|<3} \mathbb{E} [H_{i\ell} H_{j\ell}] \\ &= \frac{n(n-1)(n-2)}{n^3} \mathbb{E} [H_{12} H_{13}] + \left(1 - \frac{n(n-1)(n-2)}{n^3} \right) q, \end{aligned}$$

where q is the appropriately-weighted mean of the various $\mathbb{E}[H_{i\ell}H_{j\ell}]$ terms for which i, j, ℓ are not mutually distinct. Since $|H_{ij}| \leq 4\nu$, $\mathbb{E}[H_{i\ell}H_{j\ell}] < 16\nu^2$ and so $|q| \leq 16\nu^2$ as well. Noting that

$$\frac{n(n-1)(n-2)}{n^3} = 1 - \frac{3}{n} + \frac{2}{n^2}$$

we obtain

$$\left| \frac{1}{n^3} \sum_{ij\ell} \mathbb{E}[H_{i\ell}H_{j\ell}] - \mathbb{E}[H_{12}H_{13}] \right| = \left(\frac{3}{n} - \frac{2}{n^2} \right) |-\mathbb{E}[H_{12}H_{13}] + q| \leq \left(\frac{3}{n} - \frac{2}{n^2} \right) 32\nu^2. \quad (10)$$

The second term can be handled similarly:

$$\begin{aligned} \frac{1}{n^4} \sum_{ijab} \mathbb{E}[H_{ij}H_{ab}] &= \frac{1}{n^4} \sum_{ijab: \{i,j,a,b\}=4} \mathbb{E}[H_{ij}H_{ab}] + \frac{1}{n^4} \sum_{ijab: \{i,j,a,b\}<4} \mathbb{E}[H_{ij}H_{ab}] \\ &= \frac{n(n-1)(n-2)(n-3)}{n^4} \mathbb{E}[H_{ij}H_{ab}] + \left(1 - \frac{n(n-1)(n-2)(n-3)}{n^4} \right) r, \end{aligned}$$

where r is the appropriately-weighted mean of the non-distinct terms, $|r| \leq 16\nu^2$. For i, j, a, b all distinct, $\mathbb{E}[H_{ij}H_{ab}] = \mathbb{E}[H_{12}]^2$. Here

$$\frac{n(n-1)(n-2)(n-3)}{n^4} = \frac{(n-1)(n^2-5n+6)}{n^3} = 1 - \frac{6}{n} + \frac{11}{n^2} - \frac{6}{n^3}$$

and so

$$\left| \frac{1}{n^4} \sum_{ijab} \mathbb{E}[H_{ij}H_{ab}] - \mathbb{E}[H_{12}]^2 \right| \leq \left(\frac{6}{n} - \frac{11}{n^2} + \frac{6}{n^3} \right) 32\nu^2. \quad (11)$$

Recalling $\sigma_k^2 = 4(\mathbb{E}[H_{12}H_{13}] - \mathbb{E}[H_{12}]^2)$,

$$|\mathbb{E} \hat{\sigma}_k^2 - \sigma_k^2| \leq 128\nu^2 \left(\frac{9}{n} - \frac{13}{n^2} + \frac{6}{n^3} \right),$$

and since $n \geq 1$, we have $13/n^2 > 6/n^3$, yielding the result. \square

Lemma 19. Under Assumptions (A) and (C), we have

$$\sup_{\omega, \omega' \in \Omega} \frac{|\hat{\sigma}_\omega^2 - \hat{\sigma}_{\omega'}^2|}{\|\omega - \omega'\|} \leq 256L_k\nu \quad \text{and} \quad \sup_{\omega, \omega' \in \Omega} \frac{|\sigma_\omega^2 - \sigma_{\omega'}^2|}{\|\omega - \omega'\|} \leq 256L_k\nu.$$

Proof. We first handle the change in $\hat{\sigma}_k$:

$$\begin{aligned} |\hat{\sigma}_{k\omega}^2 - \hat{\sigma}_{k\omega'}^2| &= 4 \left| \frac{1}{n^3} \sum_{ij\ell} H_{i\ell}^{(\omega)} H_{j\ell}^{(\omega)} - \frac{1}{n^3} \sum_{ij\ell} H_{i\ell}^{(\omega')} H_{j\ell}^{(\omega')} - \frac{1}{n^4} \sum_{ijab} H_{ij}^{(\omega)} H_{ab}^{(\omega)} + \frac{1}{n^4} \sum_{ijab} H_{ij}^{(\omega')} H_{ab}^{(\omega')} \right| \\ &\leq \frac{4}{n^3} \sum_{ij\ell} |H_{i\ell}^{(\omega)} H_{j\ell}^{(\omega)} - H_{i\ell}^{(\omega')} H_{j\ell}^{(\omega')}| + \frac{4}{n^4} \sum_{ijab} |H_{ij}^{(\omega)} H_{ab}^{(\omega)} - H_{ij}^{(\omega')} H_{ab}^{(\omega')}|. \end{aligned}$$

We can handle both terms by bounding

$$\begin{aligned} |H_{ij}^{(\omega)} H_{ab}^{(\omega)} - H_{ij}^{(\omega')} H_{ab}^{(\omega')}| &\leq |H_{ij}^{(\omega)} H_{ab}^{(\omega)} - H_{ij}^{(\omega)} H_{ab}^{(\omega')}| + |H_{ij}^{(\omega)} H_{ab}^{(\omega')} - H_{ij}^{(\omega')} H_{ab}^{(\omega')}| \\ &= |H_{ij}^{(\omega)}| |H_{ab}^{(\omega)} - H_{ab}^{(\omega')}| + |H_{ij}^{(\omega)} - H_{ij}^{(\omega')}| |H_{ab}^{(\omega')}| \\ &\leq 4\nu \left(|H_{ab}^{(\omega)} - H_{ab}^{(\omega')}| + |H_{ij}^{(\omega)} - H_{ij}^{(\omega')}| \right). \end{aligned}$$

Using Assumption (C) and the definition of H ,

$$|H_{ij}^{(\omega)} - H_{ij}^{(\omega')}| \leq 4L_k \|\omega - \omega'\|$$

so

$$|H_{ij}^{(\omega)} H_{ab}^{(\omega)} - H_{ij}^{(\omega')} H_{ab}^{(\omega')}| \leq 32\nu L_k \|\omega - \omega'\| \quad (12)$$

and hence

$$|\hat{\sigma}_\omega^2 - \hat{\sigma}_{\omega'}^2| \leq 256\nu L_k \|\omega - \omega'\|.$$

Again using (12), we also have

$$\begin{aligned} |\sigma_\omega^2 - \sigma_{\omega'}^2| &\leq 4|\mathbb{E}[H_{12}^{(\omega)} H_{13}^{(\omega)}] - \mathbb{E}[H_{12}^{(\omega')} H_{13}^{(\omega')}]| + 4|\mathbb{E}[H_{12}^{(\omega)}]^2 - \mathbb{E}[H_{12}^{(\omega')}]^2| \\ &\leq 4\mathbb{E}|H_{12}^{(\omega)} H_{13}^{(\omega)} - H_{12}^{(\omega')} H_{13}^{(\omega')}| + 4\mathbb{E}|H_{12}^{(\omega)} H_{34}^{(\omega)} - H_{12}^{(\omega')} H_{34}^{(\omega')}| \\ &\leq 256\nu L_k \|\omega - \omega'\|. \end{aligned} \quad \square$$

A.4. Constructing appropriate kernels

We now show Propositions 7 to 9, which each state that Assumption (C) is satisfied by various choices of kernel. The following assumption will be useful for different kernel schemes.

(I) The domain \mathcal{X} is Euclidean and bounded, $\mathcal{X} \subseteq \{x \in \mathbb{R}^d : \|x\| \leq R_X\}$ for some constant $R_X < \infty$.

We begin by recalling a well-known property of the Gaussian kernel, useful for both Gaussian bandwidth selection and deep kernels. A proof is in Appendix A.5.

Lemma 20. *The Gaussian kernel $\kappa(a, b) = \exp\left(-\frac{\|a-b\|^2}{2\sigma^2}\right)$ satisfies*

$$|\kappa(a, b) - \kappa(a', b')| \leq \frac{1}{\sigma\sqrt{e}} (\|a - b\| + \|a' - b'\|) \leq \frac{1}{\sigma\sqrt{e}} (\|a - a'\| + \|b - b'\|).$$

A.4.1. GAUSSIAN BANDWIDTH SELECTION (PROPOSITION 7)

Lemma 20 immediately gives us Assumption (C) when we chose among Gaussian kernels:

Proposition 21. *Define a one-dimensional Banach space for inverse lengthscales of Gaussian kernels $\gamma > 0$, so that $k_\gamma(x, y) = \kappa_{1/\gamma}(x, y)$, with standard addition and multiplication and norms defined by the absolute value, and k_0 taken to be the constant 1 function. Let Ω be any subset of this space. Under Assumption (I), Assumption (C) holds: for any $x, y \in \mathcal{X}$ and $\gamma, \gamma' \in \Gamma$,*

$$|k_\gamma(x, y) - k_{\gamma'}(x, y)| \leq \frac{2R_X}{\sqrt{e}} |\gamma - \gamma'|.$$

Proof.

$$|k_\gamma(x, y) - k_{\gamma'}(x, y)| = |\kappa_1(\gamma x, \gamma y) - \kappa_1(\gamma' x, \gamma' y)| \leq \frac{1}{\sqrt{e}} |\gamma\|x - y\| - \gamma'\|x - y\|| = \frac{\|x - y\|}{\sqrt{e}} |\gamma - \gamma'|. \quad \square$$

A.4.2. DEEP KERNELS (PROPOSITION 9)

To handle the deep kernel case, we will need some more assumptions on the form of the kernel.

(II) $\phi_\omega(x) = \phi_\omega^{(\Lambda)}$ is a feedforward neural network with Λ layers given by

$$\phi_\omega^{(0)}(x) = x \quad \phi_\omega^{(\ell)}(x) = \sigma^{(\ell)}\left(W_\omega^{(\ell)} \phi_\omega^{(\ell-1)}(x) + b_\omega^{(\ell)}\right),$$

where the network parameter ω consists of all the weight matrices $W_\omega^{(\ell)}$ and biases $b_\omega^{(\ell)}$, and the activation functions $\sigma^{(\ell)}$ are each 1-Lipschitz, $\|\sigma^{(\ell)}(x) - \sigma^{(\ell)}(y)\| \leq \|x - y\|$, with $\sigma^{(\ell)}(0) = 0$ so that $\|\sigma^{(\ell)}(x)\| \leq \|x\|$. Define a Banach space on ω , with addition and scalar multiplication componentwise, and

$$\|\omega\| = \max_{\ell \in \{1, \dots, \Lambda\}} \max\left(\|W_\omega^{(\ell)}\|, \|b_\omega^{(\ell)}\|\right),$$

where the matrix norm denotes operator norm $\|W\| = \sup_x \|Wx\|/\|x\|$. (For convolutional networks, see Remark 25.)

(III) k_ω is a kernel of the form (1),

$$k_\omega(x, y) = [(1 - \epsilon)\kappa(\phi_\omega(x), \phi_\omega(y)) + \epsilon]q(x, y),$$

with $0 \leq \epsilon \leq 1$, κ a kernel function, and $q(x, y)$ a kernel with $\sup_x q(x, x) \leq Q$.

Note that this includes kernels of the form $k_\omega(x, y) = \kappa(\phi_\omega(x), \phi_\omega(y))$: take $\epsilon = 0$ and $q(x, y) = 1$.

(IV) κ in Assumption (III) is a kernel function satisfying

$$|\kappa(a, b) - \kappa(a', b')| \leq L_\kappa (\|a - a'\| + \|b - b'\|).$$

This holds for a Gaussian κ via Lemma 20.

We now turn to proving Assumption (C) for deep kernels. First, we will need some smoothness properties of the network ϕ .

Lemma 22. Under Assumption (II), suppose ω, ω' have $\|\omega\| \leq R, \|\omega'\| \leq R$, with $R \neq 1$. Then, for any x ,

$$\|\phi_\omega(x)\| \leq R^\Lambda \|x\| + \frac{R}{R-1}(R^\Lambda - 1) \quad (13)$$

$$\|\phi_\omega(x) - \phi_{\omega'}(x)\| \leq \left(\Lambda R^{\Lambda-1} \left(\|x\| + \frac{R}{R-1} \right) - \frac{R^\Lambda - 1}{(R-1)^2} \right) \|\omega - \omega'\|. \quad (14)$$

If $R \geq 2$, we furthermore have

$$\|\phi_\omega(x)\| \leq R^\Lambda (\|x\| + 2) \quad (15)$$

$$\|\phi_\omega(x) - \phi_{\omega'}(x)\| \leq \Lambda R^{\Lambda-1} (\|x\| + 2) \|\omega - \omega'\|. \quad (16)$$

The proof, by recursion, is given in Appendix A.5. We are now ready to prove Assumption (C) for deep kernels.

Proposition 23. Make Assumptions (I) to (IV) and Assumption (B), with $R_\Omega \geq 2$.⁸ Then Assumption (C) holds: for any $x, y \in \mathcal{X}$ and $\omega, \omega' \in \Omega$,

$$|k_\omega(x, y) - k_{\omega'}(x, y)| \leq 2Q(1 - \epsilon)L_\kappa \Lambda R_\Omega^{\Lambda-1}(R_X + 2)\|\omega - \omega'\|.$$

Proof.

$$\begin{aligned} |k_\omega(x, y) - k_{\omega'}(x, y)| &= (1 - \epsilon)|\kappa(\phi_\omega(x), \phi_\omega(y)) - \kappa(\phi_{\omega'}(x), \phi_{\omega'}(y))|q(x, y) \\ &\leq Q(1 - \epsilon)L_\kappa (|\phi_\omega(x) - \phi_{\omega'}(x)| + |\phi_\omega(y) - \phi_{\omega'}(y)|) \\ &\leq Q(1 - \epsilon)L_\kappa \Lambda R_\Omega^{\Lambda-1} (\|x\| + \|y\| + 4) \|\omega - \omega'\| \\ &\leq Q(1 - \epsilon)L_\kappa \Lambda R_\Omega^{\Lambda-1} (2R_X + 4) \|\omega - \omega'\|. \end{aligned} \quad \square$$

Remark 24. For the deep kernels we use in the paper (Assumptions (II) to (IV)) on bounded domains (Assumption (I)), we know L_κ via Proposition 23; Theorem 6 combines Theorem 11, Corollary 12, and Proposition 23. If we further use a Gaussian kernel q of bandwidth σ_ϕ , the last bracketed term in the error bound of Theorem 11 becomes

$$\frac{2(1 - \epsilon)}{\sigma_\phi \sqrt{e}} \Lambda R_\Omega^{\Lambda-1} (R_X + 2) + \sqrt{2 \log \frac{2}{\delta} + 2D \log(4R_\Omega \sqrt{n})}.$$

The component $R_\Omega^{\Lambda-1}(R_X + 2)$, from (15), is approximately the largest that ϕ_ω could make its outputs' norms; σ_ϕ will generally be on a comparable scale to the norm of the actual outputs of the network, so their ratio is something like the "unused capacity" of the network to blow up its inputs. This term is weighted about equally in the convergence bound with the square root of the total number of parameters in the network.

Remark 25. We can handle convolutional networks as follows. We define Ω in essentially the same way, letting $W_\omega^{(\ell)}$ denote the convolutional kernel (the set of parameters being optimized), but define $\|\omega\|$ in terms of the operator norm of the linear transform corresponding to the convolution operator. This is given in terms of the operator norm of various discrete Fourier transforms of the kernel matrix by Lemma 2 of Bibi et al. (2019); see also Theorem 6 of Sedghi et al. (2019). The number of parameters D is then the actual number of parameters optimized in gradient descent, but the radius R_Ω is computed differently.

⁸Of course, if we know a bound of $R_\Omega < 2$, the result will still hold using $R_\Omega = 2$. It is also possible to show a tighter result, via (13) and (14) or their analogue for $R = 1$; the expression is simply less compact.

A.4.3. MULTIPLE KERNEL LEARNING (PROPOSITION 8)

Multiple kernel learning (Gönen & Alpaydn, 2011) also falls into our setting. A special case of this family of kernels was studied for the (easier to analyze) “streaming” MMD estimator by Gretton et al. (2012b).

(V) Let $\{k_i\}_{i=1}^D$ be a set of base kernels, each satisfying $\sup_{x \in \mathcal{X}} k_i(x, x) \leq K$ for some finite K . Define k_ω as

$$k_\omega(x, y) = \sum_{i=1}^D \omega_i k_i(x, y).$$

Define the norm of a kernel parameter by the norm of the corresponding vector $\omega \in \mathbb{R}^D$. Let Ω be a set of possible parameters such that for each $\omega \in \Omega$, k_ω is positive semi-definite, and $\|\omega\| \leq R_\Omega$ for some $R_\Omega < \infty$.

Not only does learning in this setting work (Proposition 26), it is also – unlike the deep setting – efficient to find an exact maximizer of \hat{J}_λ (Proposition 27).

Proposition 26. *Assumption (V) implies Assumptions (A) to (C). In particular,*

$$\begin{aligned} \sup_{\omega \in \Omega} \sup_{x \in \mathcal{X}} k_\omega(x, x) &\leq K R_\Omega \sqrt{D} \\ |k_\omega(x, y) - k_{\omega'}(x, y)| &\leq K \sqrt{D} \|\omega - \omega'\|. \end{aligned}$$

Proof. Assumption (B) is immediate from Assumption (V), since $\Omega \subset \mathbb{R}^D$. Let $\mathbf{k}(x, y) \in \mathbb{R}^D$ denote the vector whose i th entry is $k_i(x, y)$, so that $k_\omega(x, y) = \omega^\top \mathbf{k}(x, y)$. As $\|\mathbf{k}(x, y)\|_\infty \leq K$, we know $\|\mathbf{k}(x, y)\| \leq K \sqrt{D}$. Assumptions (A) and (C) follow by Cauchy-Schwartz. \square

Proposition 27. *Take Assumption (V), and additionally assume that $\Omega = \{\omega \mid \forall i. \omega_i \geq 0, \sum_i \omega_i = Q\}$ for some $Q < \infty$. A maximizer of $\hat{J}_\lambda(\omega)$ can then be found by scaling the solution to a convex quadratic program,*

$$\tilde{\omega} = \arg \min_{\omega \in [0, \infty)^D : \omega^\top \mathbf{b} = 1} \omega^\top (\mathbf{A} + \lambda I) \omega, \quad \hat{\omega} = \frac{Q}{\sum_i \tilde{\omega}_i} \tilde{\omega} \in \arg \max_{\omega \in \Omega} \hat{J}_\lambda(\omega),$$

where

$$\begin{aligned} (\mathbf{H}_{ij})_\ell &= k_\ell(X_i, X_j) + k_\ell(Y_i, Y_j) - k_\ell(X_i, Y_j) - k_\ell(X_j, Y_i) \\ \mathbf{b} &= \frac{1}{n(n-1)} \sum_{i \neq j} \mathbf{H}_{ij} \in \mathbb{R}^D \\ \mathbf{A} &= \frac{4}{n^3} \sum_i \left(\sum_j \mathbf{H}_{ij} \right) \left(\sum_j \mathbf{H}_{ij} \right)^\top - \frac{4}{n^4} \left(\sum_{ij} \mathbf{H}_{ij} \right) \left(\sum_{ij} \mathbf{H}_{ij} \right)^\top \in \mathbb{R}^{D \times D}, \end{aligned}$$

as long as \mathbf{b} has at least one positive entry.

Proof. The H matrix used by $\hat{\eta}_\omega$ and $\hat{\sigma}_\omega$ takes a simple form:

$$H_{ij}^{(\omega)} = k_\omega(X_i, X_j) + k_\omega(Y_i, Y_j) - k_\omega(X_i, Y_j) - k_\omega(X_j, Y_i) = \omega^\top \mathbf{H}_{ij}.$$

Thus

$$\begin{aligned} \hat{\eta}_\omega &= \omega^\top \left(\frac{1}{n(n-1)} \sum_{i \neq j} \mathbf{H}_{ij} \right) = \omega^\top \mathbf{b} \\ \hat{\sigma}_\omega^2 &= \frac{4}{n^3} \sum_i \left(\omega^\top \sum_j \mathbf{H}_{ij} \right)^2 - \frac{4}{n^4} \left(\omega^\top \sum_{ij} \mathbf{H}_{ij} \right)^2 \\ &= \omega^\top \left(\frac{4}{n^3} \sum_i \left(\sum_j \mathbf{H}_{ij} \right) \left(\sum_j \mathbf{H}_{ij} \right)^\top - \frac{4}{n^4} \left(\sum_{ij} \mathbf{H}_{ij} \right) \left(\sum_{ij} \mathbf{H}_{ij} \right)^\top \right) \omega = \omega^\top \mathbf{A} \omega. \end{aligned}$$

Note that because $\hat{\sigma}_\omega^2 \geq 0$ for any ω , we have $\mathbf{A} \succeq 0$. We have now obtained a problem equivalent to the one in Section 4 of [Gretton et al. \(2012b\)](#); the argument proceeds as there. \square

A.5. Miscellaneous Proofs

The following lemma was used for Propositions 21 and 23.

Lemma 20. *The Gaussian kernel $\kappa(a, b) = \exp\left(-\frac{\|a-b\|^2}{2\sigma^2}\right)$ satisfies*

$$|\kappa(a, b) - \kappa(a', b')| \leq \frac{1}{\sigma\sqrt{e}} (\|a - b\| + \|a' - b'\|) \leq \frac{1}{\sigma\sqrt{e}} (\|a - a'\| + \|b - b'\|).$$

Proof. We have that

$$\begin{aligned} |\kappa(a, b) - \kappa(a', b')| &= \left| \exp\left(-\frac{\|a-b\|^2}{2\sigma^2}\right) - \exp\left(-\frac{\|a'-b'\|^2}{2\sigma^2}\right) \right| \\ &\leq \|x \mapsto \exp\left(-\frac{x^2}{2\sigma^2}\right)\|_L \|a - b\| - \|a' - b'\|. \end{aligned}$$

We can bound the Lipschitz constant as its maximal derivative norm,

$$\sup_x \frac{|x|}{\sigma^2} \exp\left(-\frac{x^2}{2\sigma^2}\right).$$

Noting that

$$\frac{d}{dx} \log\left(\frac{|x|}{\sigma^2} \exp\left(-\frac{x^2}{2\sigma^2}\right)\right) = \frac{1}{x} - \frac{x}{\sigma^2}$$

vanishes only at $x = \pm\sigma$, the supremum is achieved by using that value, giving

$$\|x \mapsto \exp\left(-\frac{x^2}{2\sigma^2}\right)\|_L = \frac{1}{\sigma\sqrt{e}}.$$

The result follows from

$$\| \|a - b\| - \|a' - b'\| \| \leq \|a - b - a' + b'\| \leq \|a - a'\| + \|b - b'\|. \quad \square$$

This next lemma was used in Proposition 23.

Lemma 22. *Under Assumption (II), suppose ω, ω' have $\|\omega\| \leq R, \|\omega'\| \leq R$, with $R \neq 1$. Then, for any x ,*

$$\|\phi_\omega(x)\| \leq R^\Lambda \|x\| + \frac{R}{R-1} (R^\Lambda - 1) \quad (13)$$

$$\|\phi_\omega(x) - \phi_{\omega'}(x)\| \leq \left(\Lambda R^{\Lambda-1} \left(\|x\| + \frac{R}{R-1} \right) - \frac{R^\Lambda - 1}{(R-1)^2} \right) \|\omega - \omega'\|. \quad (14)$$

If $R \geq 2$, we furthermore have

$$\|\phi_\omega(x)\| \leq R^\Lambda (\|x\| + 2) \quad (15)$$

$$\|\phi_\omega(x) - \phi_{\omega'}(x)\| \leq \Lambda R^{\Lambda-1} (\|x\| + 2) \|\omega - \omega'\|. \quad (16)$$

Proof. First, $\|\phi_\omega^{(0)}(x)\| = \|x\|$, showing (13) when $\Lambda = 0$. In general,

$$\begin{aligned} \|\phi_\omega^{(\ell)}(x)\| &= \|\sigma^{(\ell)} \left(W_\omega^{(\ell)} \phi_\omega^{(\ell-1)}(x) + b_\omega^{(\ell)} \right)\| \\ &\leq \|W_\omega^{(\ell)} \phi_\omega^{(\ell-1)}(x) + b_\omega^{(\ell)}\| \\ &\leq \|W_\omega^{(\ell)}\| \|\phi_\omega^{(\ell-1)}(x)\| + \|b_\omega^{(\ell)}\| \\ &\leq R \|\phi_\omega^{(\ell-1)}(x)\| + R, \end{aligned}$$

and expanding this recursion gives

$$\|\phi_\omega^{(\ell)}(x)\| \leq R^\ell \|x\| + \sum_{m=1}^{\ell} R^m = R^\ell \|x\| + \frac{R}{R-1}(R^\ell - 1).$$

Now, we have (14) for $\Lambda = 0$ because $\phi_\omega^{(0)}(x) - \phi_{\omega'}^{(0)}(x) = 0$. For $\ell \geq 1$, we have

$$\begin{aligned} \|\phi_\omega^{(\ell)}(x) - \phi_{\omega'}^{(\ell)}(x)\| &= \|\sigma^{(\ell)} \left(W_\omega^{(\ell)} \phi_\omega^{(\ell-1)}(x) + b_\omega^{(\ell)} \right) - \sigma^{(\ell)} \left(W_{\omega'}^{(\ell)} \phi_{\omega'}^{(\ell-1)}(x) + b_{\omega'}^{(\ell)} \right)\| \\ &\leq \|W_\omega^{(\ell)} \phi_\omega^{(\ell-1)}(x) - W_{\omega'}^{(\ell)} \phi_\omega^{(\ell-1)}(x)\| + \|W_{\omega'}^{(\ell)} \phi_\omega^{(\ell-1)}(x) - W_{\omega'}^{(\ell)} \phi_{\omega'}^{(\ell-1)}(x)\| + \|b_\omega^{(\ell)} - b_{\omega'}^{(\ell)}\| \\ &\leq \|W_\omega^{(\ell)} - W_{\omega'}^{(\ell)}\| \|\phi_\omega^{(\ell-1)}(x)\| + \|W_{\omega'}^{(\ell)}\| \|\phi_\omega^{(\ell-1)}(x) - \phi_{\omega'}^{(\ell-1)}(x)\| + \|\omega - \omega'\| \\ &\leq \|\omega - \omega'\| \left(R^{\ell-1} \|x\| + \frac{R}{R-1}(R^{\ell-1} - 1) + 1 \right) + R \|\phi_\omega^{(\ell-1)}(x) - \phi_{\omega'}^{(\ell-1)}(x)\|. \end{aligned}$$

Expanding the recursion yields

$$\begin{aligned} \|\phi_\omega^{(\ell)}(x) - \phi_{\omega'}^{(\ell)}(x)\| &\leq \sum_{m=0}^{\ell-1} R^m \left(R^{\ell-1-m} \|x\| + \frac{R}{R-1}(R^{\ell-m-1} - 1) + 1 \right) \|\omega - \omega'\| \\ &= \sum_{m=0}^{\ell-1} \left(R^{\ell-1} \|x\| + \frac{R^\ell}{R-1} - \frac{R^{m+1}}{R-1} + R^m \right) \|\omega - \omega'\| \\ &= \left(\ell R^{\ell-1} \|x\| + \frac{\ell R^\ell}{R-1} - \left(\frac{R}{R-1} - 1 \right) \sum_{m=0}^{\ell-1} R^m \right) \|\omega - \omega'\| \\ &= \left(\ell R^{\ell-1} \left(\|x\| + \frac{R}{R-1} \right) - \frac{1}{R-1} \frac{R^\ell - 1}{R-1} \right) \|\omega - \omega'\|. \end{aligned}$$

When $R \geq 2$, we have that $R/(R-1) \leq 2$ and $R^\ell > 1$, giving (15) and (16). \square

B. Experimental Details

B.1. Details of synthetic datasets

Table 6 shows details of four synthetic datasets. *Blob* datasets are often used to validate two-sample test methods (Gretton et al., 2012b; Jitkrittum et al., 2016; Sutherland et al., 2017), although we rotate each blob to show the benefits of non-homogeneous kernels. *HDGM* datasets are first proposed in this paper. *HDGM-D* can be regarded as *high-dimension Blob-D* which contains two modes with the same variance and different covariance.

Table 6. Specifications of \mathbb{P} and \mathbb{Q} of synthetic datasets. $\mu_1^b = [0, 0]$, $\mu_2^b = [0, 1]$, $\mu_3^b = [0, 2]$, \dots , $\mu_8^b = [2, 1]$, $\mu_9^b = [2, 2]$ (same with Figure 1a). $\mu_1^h = \mathbf{0}_d$, $\mu_2^h = 0.5 \times \mathbf{1}_d$, I_d is an identity matrix with size d . $\Delta_i^b = -0.02 - 0.002 \times (i - 1)$ if $i < 5$ and $\Delta_i^b = 0.02 + 0.002 \times (i - 6)$ if $i > 5$. if $i = 5$, $\Delta_i^b = 0$ (same with Figure 1a). Δ_1^h and Δ_2^h are set to 0.5 and -0.5 , respectively.

Datasets	\mathbb{P}	\mathbb{Q}
<i>Blob-S</i>	$\sum_{i=1}^9 \frac{1}{9} \mathcal{N}(\mu_i^b, 0.03 \times I_2)$	$\sum_{i=1}^9 \frac{1}{9} \mathcal{N}(\mu_i^b, 0.03 \times I_2)$
<i>Blob-D</i>	$\sum_{i=1}^9 \frac{1}{9} \mathcal{N}(\mu_i^b, 0.03 \times I_2)$	$\sum_{i=1}^9 \frac{1}{9} \mathcal{N} \left(\mu_i^b, \begin{bmatrix} 0.03 & \Delta_i^b \\ \Delta_i^b & 0.03 \end{bmatrix} \right)$
<i>HDGM-S</i>	$\sum_{i=1}^2 \frac{1}{2} \mathcal{N}(\mu_i^h, I_d)$	$\sum_{i=1}^2 \frac{1}{2} \mathcal{N}(\mu_i^h, I_d)$
<i>HDGM-D</i>	$\sum_{i=1}^2 \frac{1}{2} \mathcal{N}(\mu_i^h, I_d)$	$\sum_{i=1}^2 \frac{1}{2} \mathcal{N} \left(\mu_i^h, \begin{bmatrix} 1 & \Delta_i^h & \mathbf{0}_{d-2} \\ \Delta_i^h & 1 & \mathbf{0}_{d-2} \\ \mathbf{0}_{d-2}^T & \mathbf{0}_{d-2}^T & I_{d-2} \end{bmatrix} \right)$

B.2. Dataset visualization

Figure 4 shows images from real-*MNIST* and “fake”-*MNIST*, while Figure 5 shows samples from *CIFAR-10* and *CIFAR-10.1*.

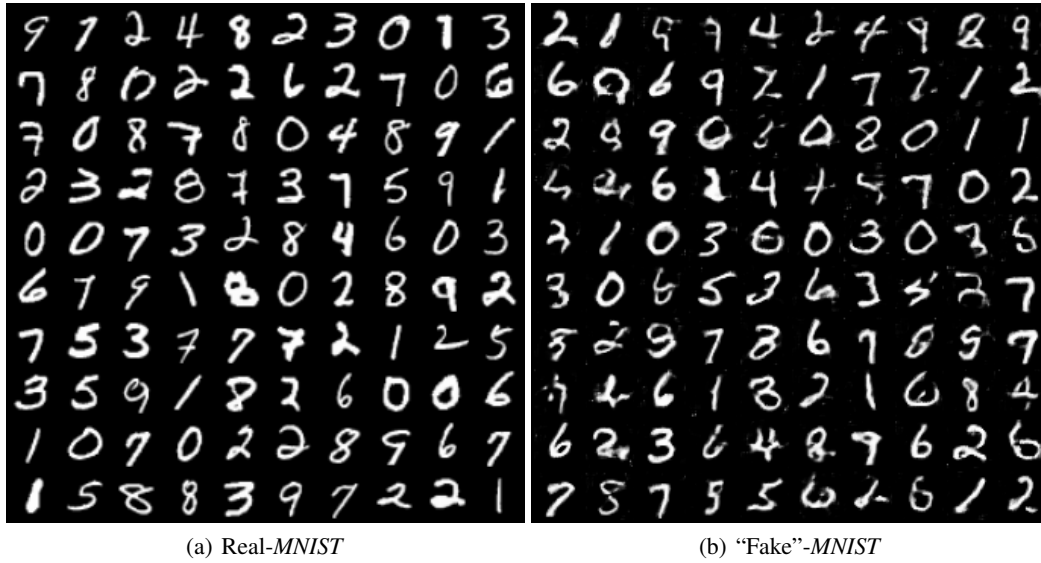


Figure 4. Images from real-*MNIST* and “fake”-*MNIST*. “Fake”-*MNIST* is generated by DCGAN (Radford et al., 2016).

B.3. Configurations

We implement all methods on Python 3.7 (Pytorch 1.1) with a NVIDIA Titan V GPU. We run ME and SCF using the official code (Jitkrittum et al., 2016), and implement C2ST-S, C2ST-L, MMD-D and MMD-O by ourselves. We use permutation test to compute p -values of C2ST-S and C2ST-L, MMD-D, MMD-O and tests in Table 4. We set $\alpha = 0.05$ for all experiments. Following Lopez-Paz & Oquab (2017), we use a deep neural network F as the classifier in C2ST-S and C2ST-L, and train the F by minimizing cross entropy. To fairly compare MMD-D with C2ST-S and C2ST-L, the network ϕ_ω in MMD-D has the same architecture with feature extractor in F . Namely, $F = g \circ \phi_\omega$, where g is a two-layer fully-connected network. The network g is a simple binary classifier that takes extracted features (through ϕ_ω) as input. For test methods shown in Table 4, the network ϕ_ω in them also has the same architecture with that in MMD-D.

For *Blob*, *HDGM* and *Higgs*, ϕ_ω is a five-layer fully-connected neural network. The number of neurons in hidden and output layers of ϕ_ω are set to 50 for *Blob*, $3 \times d$ for *HDGM* and 20 for *Higgs*, where d is the dimension of samples. These neurons are with softplus activation function, i.e., $\log(1 + \exp(x))$. For *MNIST* and *CIFAR*, ϕ_ω is a *convolutional neural network* (CNN) that contains four convolutional layers and one fully-connected layer. The structure of the CNN follows the structure of the feature extractor in the discriminator of DCGAN (Radford et al., 2016) (see Figures 6 and 8 for the structure of ϕ_ω in MMD-D, and Figures 7 and 9 for the structure of classifier F in C2ST-S and C2ST-L). The link of DCGAN code is <https://github.com/eriklindernoren/PyTorch-GAN/blob/master/implementations/dcgan/dcgan.py>.

We use Adam optimizer (Kingma & Ba, 2015) to optimize 1) parameters of F in C2ST-S and C2ST-L, 2) parameters of ϕ_ω in MMD-D and 3) kernel lengthscale in MMD-O. We set drop-out rate to zero when training C2ST-S, C2ST-L and MMD-D on all datasets.

B.4. Detailed parameters of all test methods

In this subsection, we demonstrate detailed parameters of all test methods. Except for learning rate of Adam optimizer, we use default parameters of Adam optimizer provided by Pytorch. We use one validation set (with the same size of training set) to roughly search these parameters. Using these parameters, we compute test power of each test method on 100 test sets (with the same size of training set).

For ME and SCF, we follow Chwialkowski et al. (2015) and set $J = 10$ for *Higgs*. For other datasets, we set $J = 5$.

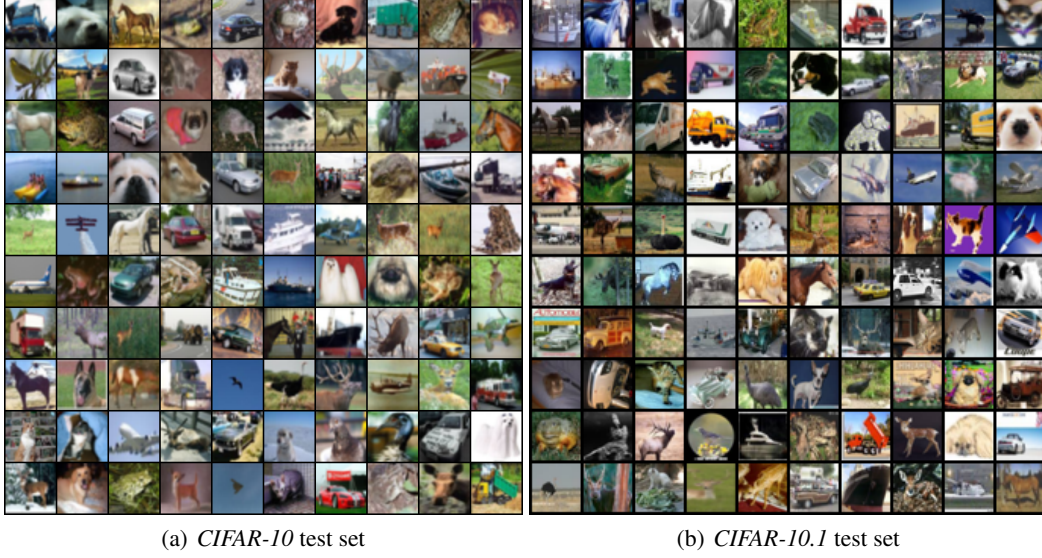


Figure 5. Images from *CIFAR-10* test set and the new *CIFAR-10.1* test set (Recht et al., 2019).

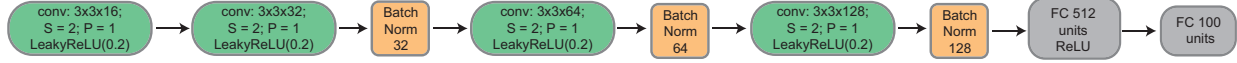


Figure 6. The structure of ϕ_ω in MMD-D on *MNIST*. The kernel size of each convolutional layer is 3; stride (S) is set to 2; padding (P) is set to 1. We do not use dropout. Best viewed zoomed in.



Figure 7. The structure of classifier F in C2ST-S and C2ST-L on *MNIST*. The kernel size of each convolutional layer is 3; stride (S) is set to 2; padding (P) is set to 1. We do not use dropout. In the first layer, we will convert the *CIFAR* images from $32 \times 32 \times 3$ to $64 \times 64 \times 3$. Best viewed zoomed in.

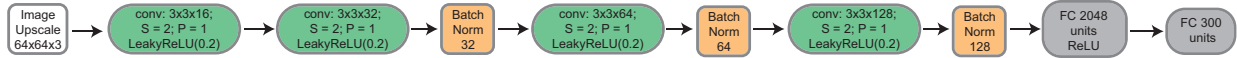


Figure 8. The structure of ϕ_ω in MMD-D on *CIFAR*. The kernel size of each convolutional layer is 3; stride (S) is set to 2; padding (P) is set to 1. We do not use dropout in all layers. In the first layer, we will convert the *CIFAR* images from $32 \times 32 \times 3$ to $64 \times 64 \times 3$. Best viewed zoomed in.



Figure 9. The structure of classifier F in C2ST-S and C2ST-L on *CIFAR*. The kernel size of each convolutional layer is 3; stride (S) is set to 2; padding (P) is set to 1. We do not use dropout. Best viewed zoomed in.

For C2ST-S and C2ST-L, we set batchsize to $\min\{2 \times n_b, 128\}$ for *Blob*, 128 for *HDGM* and *Higgs*, and 100 for *MNIST* and *CIFAR*. We set the number of epochs to $500 \times 18 \times n_b / \text{batchsize}$ for *Blob*, 1,000 for *HDGM*, *Higgs* and *CIFAR*, and 2,000 for *MNIST*. We set learning rate to 0.001 for *Blob*, *HDGM* and *Higgs*, and 0.0002 for *MNIST* and *CIFAR* (following Radford et al. (2016)).

For MMD-O, we use full batch (i.e., all samples) to train MMD-O. we set the number of epochs to 1,000 for *Blob*, *HDGM*, *Higgs* and *CIFAR*, and 2,000 for *MNIST*. We set learning rate to 0.0005 for *Blob*, *MNIST* and *CIFAR*, and 0.001 for *HDGM*.

Table 7. Results on *Higgs* ($\alpha = 0.05$). We report average Type I error on *Higgs* dataset when increasing number of samples (N). Note that, in *Higgs*, we have two types of Type I errors: 1) Type I error when two samples drawn from \mathbb{P} (no Higgs bosons) and 2) Type I error when two samples drawn from \mathbb{Q} (having Higgs bosons). Type I reported here is the average value of 1) and 2). Since Type I error reported here is the average value of two average Type I errors, we do not report standard errors of the average Type I error in this table.

N	ME	SCF	C2ST-S	C2ST-L	MMD-O	MMD-D
1000	0.048	0.040	0.043	0.048	0.059	0.037
2000	0.043	0.032	0.060	0.056	0.055	0.053
3000	0.049	0.043	0.046	0.053	0.051	0.069
5000	0.056	0.035	0.052	0.065	0.049	0.062
8000	0.050	0.034	0.065	0.067	0.056	0.037
10000	0.059	0.032	0.057	0.058	0.045	0.048
Avg.	0.051	0.036	0.054	0.058	0.050	0.051

Table 8. Results on *MNIST* given $\alpha = 0.05$. We report average Type I error \pm standard errors on real-*MNIST* vs. real-*MNIST* when increasing number of samples (N).

N	ME	SCF	C2ST-S	C2ST-L	MMD-O	MMD-D
200	0.076 \pm 0.011	0.075 \pm 0.010	0.035 \pm 0.006	0.045 \pm 0.005	0.068 \pm 0.004	0.056 \pm 0.003
400	0.062 \pm 0.010	0.056 \pm 0.007	0.044 \pm 0.006	0.040 \pm 0.004	0.053 \pm 0.005	0.056 \pm 0.005
600	0.051 \pm 0.003	0.049 \pm 0.009	0.039 \pm 0.005	0.054 \pm 0.007	0.066 \pm 0.008	0.056 \pm 0.008
800	0.054 \pm 0.006	0.046 \pm 0.006	0.043 \pm 0.005	0.042 \pm 0.007	0.051 \pm 0.005	0.054 \pm 0.007
1000	0.047 \pm 0.006	0.045 \pm 0.010	0.038 \pm 0.006	0.046 \pm 0.005	0.041 \pm 0.007	0.062 \pm 0.006
Avg.	0.058	0.054	0.040	0.045	0.056	0.057

For MMD-D, we use full batch (i.e., all samples) to train MMD-D with samples from *Blob*, *HDGM* and *Higgs*. We use mini-batch (batchsize is 100) to train MMD-D with samples from *MNIST* and *CIFAR*. We set the number of epochs to 1,000 for *Blob*, *HDGM*, *Higgs* and *CIFAR*, and 2,000 for *MNIST*. We set learning rate to 0.0005 for *Blob* and *Higgs*, 10^{-5} for *HDGM*, 0.001 for *MNIST* and 0.0002 for *CIFAR* (following Radford et al. (2016)).

B.5. Links to datasets

Higgs dataset can be downloaded from UCI Machine Learning Repository. The link is <https://archive.ics.uci.edu/ml/datasets/HIGGS>.

MNIST dataset can be downloaded via Pytorch. See the code in <https://github.com/eriklindernoren/PyTorch-GAN/blob/master/implementations/dcgan/dcgan.py>.

CIFAR-10.1 is available from <https://github.com/modestyachts/CIFAR-10.1/tree/master/datasets> (we use `cifar10.1.v4_data.npy`). This new test set contains 2,031 images from TinyImages (Torrallba et al., 2008).

B.6. Type I errors on *Higgs* and *MNIST*

Table 7 shows average Type I error on *Higgs* dataset when increasing number of samples (N). Table 8 shows average Type I error on real-*MNIST* vs. real-*MNIST* when increasing number of samples (N).

C. Interpretability on *CIFAR-10* vs *CIFAR-10.1*

In Section 7.1, we have shown that images in *CIFAR-10* and *CIFAR-10.1* are not from the same distribution. Thus, it is interesting to try to understand the major difference between the datasets. Mean Embedding tests (Chwialkowski et al., 2015) compare the mean embeddings $\mu_{\mathbb{P}}$ and $\mu_{\mathbb{Q}}$ at test locations v_1, \dots, v_L , rather than through their overall norm. The test statistic is

$$\hat{\Lambda} = n \bar{z}_n^T S^{-1} \bar{z}_n, \quad z_i = (k(x_i, v_j) - k(y_i, v_j))_{j=1}^L \in \mathbb{R}^L, \quad \bar{z}_n = \frac{1}{n} \sum_{i=1}^n z_i, \quad S_n = \frac{1}{n-1} \sum_{i=1}^n (z_i - \bar{z}_n)(z_i - \bar{z}_n)^T;$$

the asymptotic null distribution of $\hat{\Lambda}$ is χ_L^2 , and the estimator is computable in linear time rather than $\widehat{\text{MMD}}_U$'s quadratic time.

Jitkrittum et al. (2017) jointly learn the parameters v_j and kernel parameters to optimize test power. The best such test locations ($L = 1$) for a Gaussian kernel (with learned bandwidth) are shown in Figure 10. We could also try optimizing a deep kernel (1) and the test locations together; this procedure, however, failed to find a useful test. We can find a better test, though, with a two-stage scheme: first, learn a deep kernel to maximize \hat{J}_λ , then choose v_i to maximize $\hat{\Lambda}$ with that kernel fixed. Results are shown in Figure 11.

Although these approaches give nontrivial test power, it is hard to interpret either set of images, as the test locations have moved far outside the set of natural images. We can instead constrain $v_1 \in S_{\mathbb{P}} \cup S_{\mathbb{Q}}$, simply picking the single point from the dataset which maximizes $\hat{\Lambda}$ (shown in Figure 12). This achieves similar test power, but lets us see that the difference might lie in images with smaller objects of interest than the mean for *CIFAR-10*.

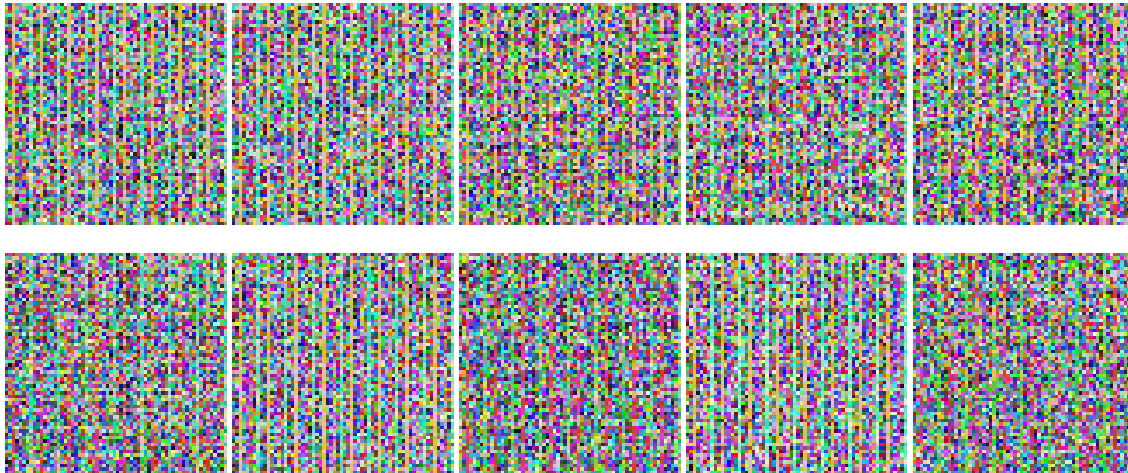


Figure 10. The best test locations (learned by an ME test with $L = 1$) from 10 experiments on *CIFAR-10* vs *CIFAR-10.1*. Average rejection rate is 0.415.

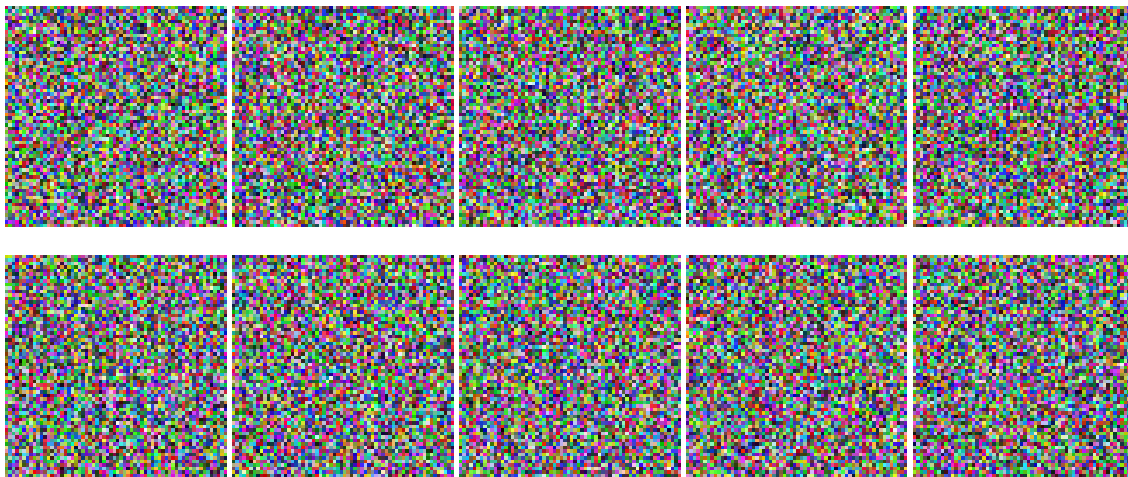


Figure 11. The best test locations (learned by an ME test, $L = 1$, with a deep kernel optimized for an MMD test) from 10 experiments on *CIFAR-10* vs *CIFAR-10.1*. Average rejection rate is 0.637.

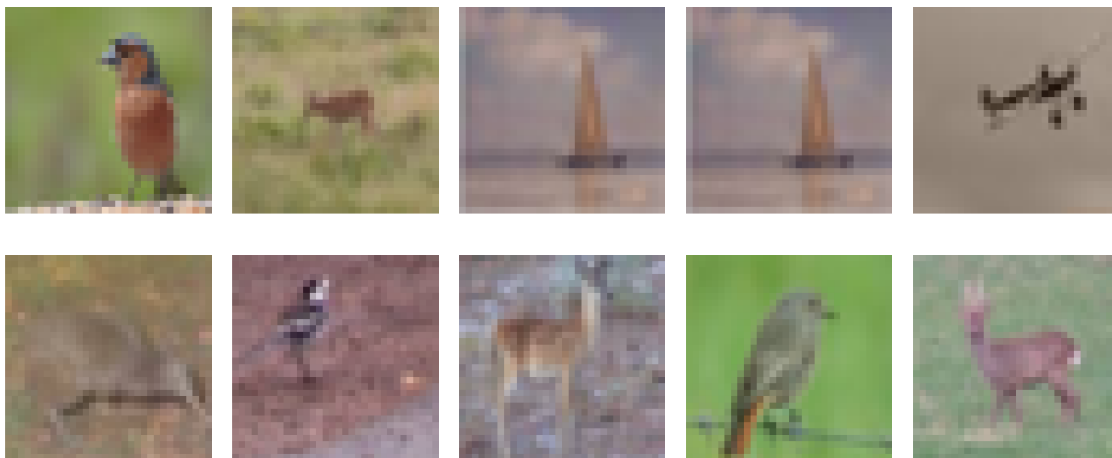


Figure 12. The best test locations (selected among existing images with our learned deep kernel, $L = 1$) from 10 experiments on *CIFAR-10* vs *CIFAR-10.1*. Average rejection rate is 0.653.